Atmos. Chem. Phys., 21, 1815–1834, 2021
https://doi.org/10.5194/acp-21-1815-2021

Atmospheric Chemistry and Physics
Open Access
EGU

$PM_{2.5}$ surface concentrations in southern West African urban areas based on sun photometer and satellite observations

Jean-François Léon[1], Aristide Barthélémy Akpo[2], Mouhamadou Bedou[3], Julien Djossou[2], Marleine Bodjrenou[2], Véronique Yoboué[3], and Cathy Liousse[1]

[1]Laboratoire d'Aérologie, Université Paul Sabatier, CNRS, Toulouse, France
[2]Laboratoire de Physique du Rayonnement, Université d'Abomey Calavi, BP 526, Cotonou, Benin
[3]Laboratoire de Physique de l'atmosphère, Université Félix-Houphouët-Boigny, Abidjan, Côte d'Ivoire

Correspondence: Jean-François Léon (jean-francois.leon@aero.obs-mip.fr)

Received: 19 June 2020 – Discussion started: 11 August 2020
Revised: 25 November 2020 – Accepted: 28 December 2020 – Published: 10 February 2021

Abstract. Southern West Africa (SWA) is influenced by large numbers of aerosol particles of both anthropogenic and natural origins. Anthropogenic aerosol emissions are expected to increase in the future due to the economical growth of African megacities. In this paper, we investigate the aerosol optical depth (AOD) in the coastal area of the Gulf of Guinea using sun photometer and MODIS satellite observations. A network of lightweight handheld sun photometers have been deployed in SWA from December 2014 to April 2017 at five different locations in Côte d'Ivoire and Benin. The handheld sun photometer measures the solar irradiance at 465, 540 and 619 nm and is operated manually once per day. Handheld-sun-photometer observations are complemented by available AERONET sun photometer observations and MODIS level 3 time series between 2003 and 2019. MODIS daily level 3 AOD agrees well with sun photometer observations in Abidjan and Cotonou (correlation coefficient $R = 0.89$ and RMSE $= 0.19$). A classification based on the sun photometer AOD and Ångström exponent (AE) is used to separate the influence of coarse mineral dust and urban-like aerosols. The AOD seasonal pattern is similar for all the sites and is clearly influenced by the mineral dust advection from December to May. Sun photometer AODs are analyzed in coincidence with surface $PM_{2.5}$ concentrations to infer trends in the particulate pollution levels over conurbations of Abidjan (Côte d'Ivoire) and Cotonou (Benin). $PM_{2.5}$-to-AOD conversion factors are evaluated as a function of the season and the aerosol type identified in the AE classification. The highest $PM_{2.5}$ concentrations (up to 300 $\mu g\,m^{-3}$) are associated with the advection of mineral dust in the heart of the dry season (December–February). Annual means are around 30 $\mu g\,m^{-3}$, and 80 % of days in the winter dry season have a value above 35 $\mu g\,m^{-3}$, while concentrations remain below 16 $\mu g\,m^{-3}$ from May to September. No obvious trend is observed in the 2003–2019 MODIS-derived $PM_{2.5}$ time series. However the short dry period (August–September), when urban-like aerosols dominate, is associated with a monotonic trend between 0.04 and 0.43 $\mu g\,m^{-3}\,yr^{-1}$ in the $PM_{2.5}$ concentrations over the period 2003–2017. The monotonic trend remains uncertain but is coherent with the expected increase in combustion aerosol emissions in SWA.

1 Introduction

The increasing trend in the anthropogenic emissions in Africa (Liousse et al., 2014) gives rise to the question of the impact of human activities on air quality, the monsoon system and the regional climate. The Gulf of Guinea and adjacent countries, hereinafter called southern West Africa (SWA), are influenced by large numbers of aerosol particles of both anthropogenic and natural origins advected from the African continent. The season cycle in SWA is driven by the monsoon system (Knippertz et al., 2015) with the alternation of a major winter (November to March) dry season and a summer (June–July) rainy season. The intertropical front (Lélé and Lamb, 2010) is at its southernmost position during the winter dry season, enabling the northeasterly Harmattan wind to carry a dust-laden dry air southward (Adetunji et al., 1979). The major conurbations of SWA are then

downwind of the mineral dust emission of the Bodélé depression in Chad, the predominant dust emission source of West Africa (Todd et al., 2007; Washington, 2005; Koren et al., 2006; Schepanski et al., 2009). Carbonaceous aerosols that are emitted by open biomass burning (Liousse et al., 2010) are also advected southward to the main coastal cities of SWA during the dry period. The summer wet season corresponds to the continental intrusion of the southwesterly monsoon winds carrying moist air and precipitation. During this period, biomass-burning emissions in central Africa can be advected to SWA by easterly wind and thus can impact the local air quality of coastal conurbations (Menut et al., 2018).

SWA is a hot spot of atmospheric aerosol concentrations as revealed by satellite-derived aerosol optical depth (Kaufman et al., 2002; Mehta et al., 2018). Atmospheric aerosols can alter the development of monsoons by weakening the land–ocean thermal contrast as well as the thermodynamic stability and the convective potential of the lower atmosphere (Li et al., 2016). Precipitation reduction in the West African monsoon region (Janicot, 1992) has been attributed to high aerosol concentrations near the Gulf of Guinea (Huang et al., 2009). Yoon et al. (2016) have pointed out the role of carbonaceous aerosols on rainfall reduction in the West African monsoon region. Aerosol effects on regional climate fall into two categories (Boucher et al., 2013). Direct effects refer to the influence of aerosol scattering and absorption on the atmospheric radiative balance. Indirect and semi-direct effects refer to the impact of aerosol on cloud properties with subsequent effects on the radiative balance. The aerosol optical depth (AOD) is one of the key parameters for assessing the aerosol direct radiative impact (Liou, 2002).

AOD is the primary aerosol optical parameter derived from satellite remote sensing (Kaufman et al., 1997). AOD is related to the reduction in the atmospheric transmission due to aerosol particles in suspension in the atmosphere. AOD can be measured directly from the ground by using a sun photometer (Volz, 1959; Prospero et al., 1979; Tanré et al., 1988; Nakajima et al., 1996). The Aerosol Robotic Network (Holben et al., 1998, 2001) is one of the most important federated network of ground-based automatic sun photometers providing continuous AOD measurements in many places of the world. West Africa benefits from a good geographical coverage of AERONET sun photometers in the Sahel transect. The stations are located in remote places dedicated to the monitoring of Saharan dust or biomass-burning-aerosol optical properties and atmospheric transport (Tanré et al., 1988; Redelsperger et al., 2006; Mallet et al., 2008; Léon et al., 2009). However sun photometer observations in the large conurbations surrounding the Gulf of Guinea remain scarce. AOD observations in the coastal part of SWA will thus provide additional ground truths for satellite validation.

Long-term satellite-derived AOD can also make up for the lack of in situ particulate matter (PM) surface observations. As air quality in SWA conurbations is still poorly covered by operational observational networks, satellite-derived PM may have a significant added value for air quality monitoring. There is abundant literature on linking columnar satellite AOD to PM (Kacenelenbogen et al., 2006; Hoff and Christopher, 2009; Ma et al., 2015; van Donkelaar et al., 2016). The relationship between instantaneous AOD and PM measurements is not straightforward, and several regression models have been tested, either linear (Kacenelenbogen et al., 2006), multi-linear (Gupta and Christopher, 2009) or nonlinear (Gupta and Christopher, 2009; Yahi et al., 2013; Kamarul Zaman et al., 2017). The conversion model from AOD to PM depends on the aerosol physical properties (aerosol type), hygroscopicity and the atmospheric dynamics, including boundary layer mixing. In particular, the variability in the planetary boundary layer depth can act as a controlling factor to the ratio between surface PM and columnar AOD (Boyouk et al., 2010; Sayer et al., 2016). Vertical profile of aerosols and meteorological parameters affect the correlation between PM and AOD (Sinha et al., 2015). Additional local analysis of the PM-to-AOD relationship based on in situ observations will strengthen the systematic retrieval of PM for satellite remote sensing.

In a companion paper (Djossou et al., 2018), the AOD measurements obtained in the downtowns of the major cities of Abidjan (Côte d'Ivoire) and Cotonou (Benin) were presented along with the surface observations of the $PM_{2.5}$ mass concentration and carbonaceous aerosol composition. A tentative analysis of the relationship between AOD and $PM_{2.5}$ was made and shows the potential of AOD to infer $PM_{2.5}$ concentration in both conurbations. In this paper, we report additional AOD measurements over SWA using lightweight handheld and automatic sun photometers with the purpose of validating the MODIS-derived AOD at the regional scale and investigating further the use of AOD for local pollution assessment. Section 2 presents the data sets and the methods. Section 3 presents the sun photometer time series and the validation of the satellite AODs. The relationship between AOD and $PM_{2.5}$ is investigated in Sect. 4. The last section presents the interannual trends in $PM_{2.5}$ derived from the MODIS observations.

2 Data and method

All the observations were acquired in a geographical box ranging from approximately 4 to 9° N and 6° W to 5° E (Fig. 1). SWA has a marked latitudinal gradient in ecosystems that largely impacts the emission and deposition of particles and trace gases (Adon et al., 2010). We define SWA as delimited by the shore of the Gulf of Guinea and 9° N, in agreement with previous authors (Kniffka et al., 2019). The domain is bounded at its southern part by the Gulf of Guinea and at its northern part by the Sudanian savanna and desertic areas of the Sahel and encompasses Guinea savanna and forest ecosystems. Major conurbations are located on the shore of the Gulf of Guinea: Abidjan (Côte d'Ivoire),

Accra (Ghana), Lomé (Togo), Cotonou (Benin) and Lagos (Nigeria). We have collected observations at three coastal locations, namely Abidjan, Cotonou and Koforidua, and four inland locations, namely Savè, Lamto, Ilorin and Comoé (see Table 1 for geographical coordinates). The sites labeled Abidjan and Cotonou are respectively located downtown in the city of Abidjan (≈ 4.4 million inhabitants) and the conurbation of Cotonou ($\approx 1,7$ million inhabitants including satellite cities). The Savè site is located in the medium-sized city of Savè ($\approx 90\,000$ inhabitants). Lamto is a rural remote site located 200 km north of Abidjan. The Comoé site is located near the village of Nassian at the southern edge of La Comoé natural reserve. The Ilorin site is located at the Department of Physics on the campus of the University of Ilorin ($\approx 800\,000$ inhabitants) in Nigeria. The Koforidua site is located at the main campus of All Nations University College, about 5 km from Koforidua City ($\approx 120\,000$ inhabitants) and 50 km north of Accra, Ghana.

2.1 Sun photometers

Table 1 summarizes the location, type of instrument and observation periods. We have used different types of sun photometers, automatic and handheld. The automatic CIMEL sun photometer is the reference instrument used in the AERONET network (Holben et al., 1998) for measuring the AOD and retrieving columnar aerosol optical properties and size distribution. We have used the level 2 quality-assured daily averages processed with the version 3 of the aerosol-optical-depth algorithm (Giles et al., 2019). We used the data for Ghana (station named Koforidua_ANUC located at 6°6′ N, 0°6′ W), Nigeria (station named Ilorin located at 8°29′ N, 4°40′ E) and Côte d'Ivoire (station named Lamto located at 6°13′ N, 5°2′ W). The geophysical station of Lamto was equipped early on, in 1997–1998, then the automatic sun photometer was restored back in 2017.

Handheld sun photometers are a well-known scientific instrumentation for measuring atmospheric transmission (Porter et al., 2001; Volz, 1959, 1974). The first type of handheld photometer we used is the one manufactured by CIMEL, hereinafter called the HHC. The HHC was operated during 2 years between April 2006 and March 2008 at Lamto geophysical station. The operating wavelengths are 440, 670 and 870 nm. The second handheld sun photometer is a new lightweight instrument manufactured by TENUM (http://www.calitoo.fr, last access: 5 February 2021) and named CALITOO (Djossou et al., 2018). CALITOO operating wavelengths are 465, 540 and 619 nm. The sun photometer measures the sun irradiance at the three wavelengths, so no additional check on the AOD curvature (Kaskaoutis and Kambezidis, 2008; Sharma et al., 2014) can be applied; however the spectral consistency between the AODs (observed at 540 nm and computed using the Ångström exponent) is checked. The atmospheric optical depth is then retrieved following the Beer–Lambert law, knowing the calibration constant for each instrument and the relative air mass. The AOD is then retrieved after subtracting the Rayleigh and trace gas optical depth.

For the HHC, observations were acquired twice a day at around 09:00 and 15:00 UTC. For the CALITOO sun photometer, the observations were acquired at around 13:00 LT. The operators were asked to make measurements only when the sun was not obscured by clouds and have proceeded with a sequence of five measurements within about 15 min. The presence of sub-visible cirrus or broken clouds within the field of view induces spurious variation in the atmospheric transmission (Smirnov et al., 2000) that can be easily detected by looking at the standard deviation of the 15 min series of AOD measurements. An arbitrary threshold of 0.2 on the standard deviation has been selected to remove the cloud-contaminated observations. The diurnal variability range is expected to be less than 10 % for our site conditions (Smirnov, 2002). The sun photometer observations are reported as daily averages.

The total uncertainty in AOD for the AERONET instruments is ± 0.01 for $\lambda > 440$ nm and ± 0.02 for shorter wavelengths (Holben et al., 1998). CALITOO sun photometers were calibrated prior to the site deployment using the Langley plot method (Soufflet et al., 1992; Schmid and Wehrli, 1995) at the Izaña high-altitude observatory (Basart et al., 2009). CALITOO observations were compared to coincident AERONET observations before and after the field experiment. The total uncertainty in AOD is estimated to ± 0.02 for all the wavelengths. Post-field measurements indicate a change of about 1 % yr^{-1} in the calibration.

AOD measurements are all reported at 550 nm because this wavelength is a reference for visibility calculation (Boers et al., 2015) and satellite missions (e.g., Remer et al., 2008). The Ångström exponent (AE) (Ångström, 1961) is computed between wavelengths 465 and 619 nm for the CALITOO, 440 and 670 nm for the HHC, and 440 and 675 nm for the AERONET.

2.2 Satellite data

The Moderate Resolution Imaging Spectroradiometer (MODIS) aerosol products (Remer et al., 2005, 2008) have been widely used by the scientific community for assessing the impact of aerosols on global climate (Boucher et al., 2013) or air quality (van Donkelaar et al., 2016). The MODIS AOD is also used in operational data assimilation for weather forecast (Benedetti et al., 2009; Lynch et al., 2016). The MODIS level 2 product has a spatial resolution of 10 km × 10 km at nadir, which increases to 20 km × 40 km at the edges of the swath. The MODIS level 3 is a regular gridded product having a spatial resolution of 1° × 1°. Most of the time, the validation exercise of MODIS-derived aerosol parameters consists of a comparison between sun photometer observations and MODIS level 2 pixels co-located in space and time (Remer et al., 2020). A box of

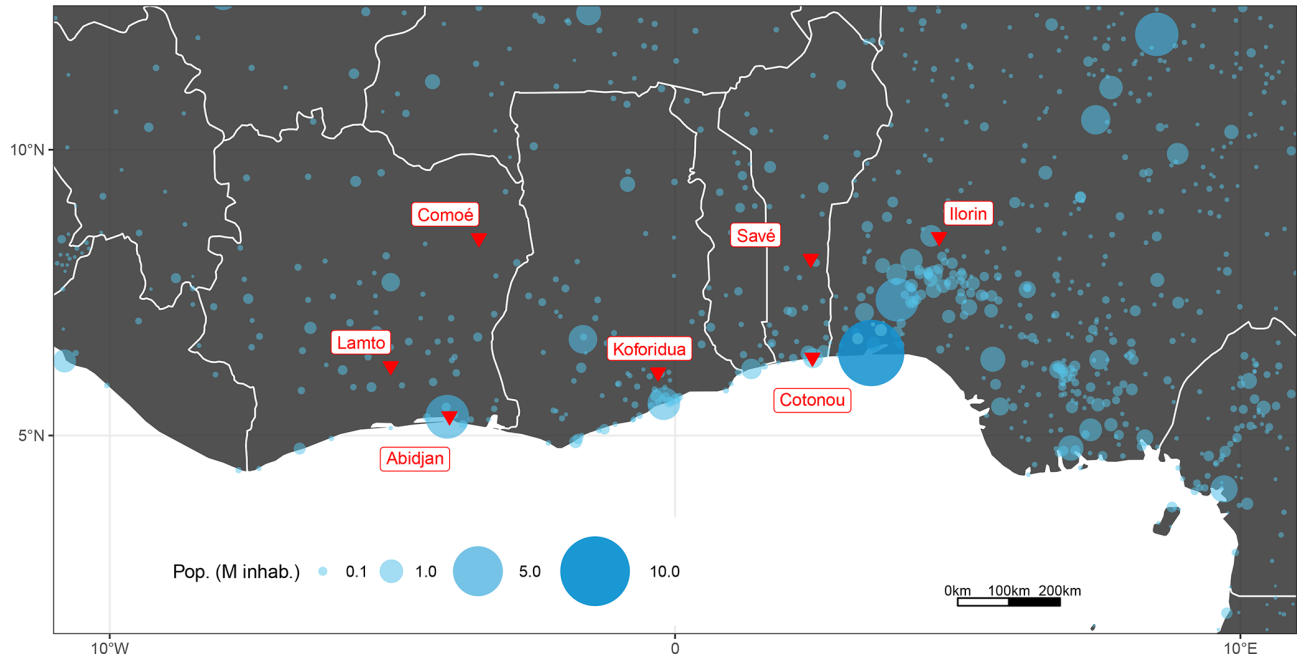

Figure 1. Map of southern West Africa (SWA) indicating the geographical locations of the sun photometer sites (red triangles) and the location and population of urban areas having more than 1000 inhabitants (blue circles with legend; source https://public.opendatasoft.com/, last access: 5 February 2021).

Table 1. Summary of observation period, number of days of observations (N) per instrument and location. Median and interquartile range (IQR) for aerosol optical depth (AOD) and Ångström exponent (AE).

Site	Type	Latitude	Longitude	Period	N	AOD median (IQR)	AE median (IQR)
Lamto	HHC	6°13′ N	5°2′ W	Mar 2006–Mar 2008	524	0.55 (0.35, 0.80)	0.68 (0.42, 0.96)
Abidjan	CALITOO	5°20′ N	3°59′ W	Feb 2015–Apr 2017	190	0.55 (0.38, 0.75)	0.73 (0.44, 0.97)
Lamto	CALITOO	6°13′ N	5°2′ W	Nov 2014–Mar 2017	499	0.47 (0.30, 0.72)	0.59 (0.35, 0.86)
Savè	CALITOO	8°01′ N	2°28′ E	Sep 2015–Oct 2017	411	0.61 (0.42, 0.86)	0.49 (0.26, 0.73)
Comoé	CALITOO	8°27′ N	3°28′ W	Jan 2016–Feb 2017	82	0.66 (0.43, 0.95)	0.33 (0.13, 0.55)
Cotonou	CALITOO	6°22′ N	2°26′ E	Nov 2014–Jun 2016	615	0.58 (0.35, 0.86)	0.58 (0.32, 0.89)
Lamto	AERONET	6°13′ N	5°2′ W	Jan 2017–Mar 2017	35	0.74 (0.59, 0.83)	0.82 (0.58, 1.08)
Ilorin	AERONET	8°29′ N	4°40′ E	Jan 2014–Mar 2017	472	0.52 (0.30, 0.89)	0.63 (0.39, 1.00)
Koforidua	AERONET	6°6′ N	0°6′ W	Dec 2015–Mar 2017	264	0.54 (0.32, 0.92)	0.78 (0.56, 1.09)

5×5 MODIS pixels and a time slot of ± 30 min around the satellite overpass is considered to be a good compromise; however the window-size dependence is small, and this compromise is more dictated by statistics rather than physics (Ichoku et al., 2002).

Gridded daily or monthly mean MODIS level 3 AODs have also been demonstrated to fit the AERONET retrievals (Ruiz-Arias et al., 2013; Wei et al., 2019). As the objective of the paper is to address the ability of MODIS data to reflect aerosol changes in a specific area rather than the validation of the retrieval algorithm, hereinafter we rely on the gridded level 3 MODIS product of the AQUA satellite (namely MYD08_D3) from 2003 to 2019. MODIS AQUA has been selected following the recommendations of Wei et al. (2019) for long-term trend analysis. This product provides several values for the AOD depending on the underlying surface and the algorithm used. For the sake of consistency between the different sites, we use the product named AOD_550_Dark_Target_Deep_Blue_Combined_Mean from version 6.1 (Levy et al., 2013) of the MODIS processing algorithm, which is a combination of the "Dark Target" (Levy et al., 2010) and "Deep Blue" (Sayer et al., 2013) methods. For the coastal sites, both AOD over land (namely Aerosol_Optical_Depth_Land_Mean or Deep_Blue_Aerosol_Optical_Depth_550_Land_Mean) and over ocean (Aerosol_Optical_Depth_Average_Ocean_Mean) are also provided. We use the "Deep Blue" AE (namely Deep_Blue_Angstrom_Exponent_Land_Mean) and com-

pute an Ångström exponent from the spectral AODs over land and ocean, respectively. For the purpose of satellite validation, the satellite AOD and AE of the nearest cell to the photometer location are extracted. We have adopted the evaluation metrics proposed by Sayer et al. (2014), including the linear correlation coefficient, the median bias, the root mean square error, the mean absolute percentage error and the fraction of data falling within the MODIS expected error (EE) given by $EE = \pm(0.05 + 0.15 \times AOD)$.

2.3 Surface concentration observations

From February 2015 to March 2017, Abidjan and Cotonou were equipped with $PM_{2.5}$ monitoring stations (Djossou et al., 2018). Particles were collected on 47 mm diameter filters (quartz and PTFE filter types) at a flow rate of $5\,L\,min^{-1}$. Samplers were equipped with a $PM_{2.5}$ mini Partisol impactor. PTFE filters were weighted before and after the sampling with a Sartorius MC21S microbalance.

The total volume of filtered air is measured by a GALLUS-type G4 gas meter. Mass concentrations of $PM_{2.5}$ are estimated from the mass load of particles on the filters and the total volume of air. The exposure duration of the filters is 1 week. A period of 1 week is sufficient to capture the main temporal pattern of atmospheric aerosols over a long period of time (Ouafo-Leumbe et al., 2017) and has been selected as a trade-off between logistics and observations.

3 Sun photometer results

3.1 Daily statistics

A total of 2323 handheld-sun-photometer observations (including data collected during the 2006 campaign) have been acquired. Starting and ending dates are reported in Table 1 along with the number of observations, median and interquartile range (IQR) of AOD and AE distributions. We select the AERONET data until the end of the CALITOO observation period, i.e., March 2017, for a total number of 1248 daily observations. There is an excellent time coverage for the stations of Lamto and Cotonou by the CALITOO observations. Observations were performed for 66 % of the time in Cotonou and 68 % in Lamto. As a comparison, this rate is 68 % for the automatic sun photometer in Koforidua, indicating that handheld measurements can be as representative as the automatic ones. This rate drops to 24 % in Abidjan and 39 % in Savè due to operating issues leading to gaps in the time series.

Considering all the stations, the AOD ranges between a minimum of 0.07 and a maximum of 3.76. The highest AOD acquired by the CALITOO instrument is 3.50 in Cotonou in March 2015, and the highest AOD recorded by the AERONET sun photometer is 3.76 in Ilorin in December 2016. The median AOD ranges between a minimum of 0.47 at Lamto and a maximum of 0.66 at Comoé. Considering all the daily measurements for all the sites, the median AOD is 0.52, and the IQR is (0.33, 0.82). AOD observations at Cotonou and Abidjan are rather similar, with a median AOD = 0.55 (0.38, 075) and 0.58 (0.35, 0.86), respectively. The observations with the automatic sun photometer in Koforidua show AOD in the same range as the two aforementioned stations, with a median AOD = 0.49 (0.33, 0.84). The observations performed at Lamto with the three kinds of sun photometers show similar AOD: 0.47 (0.3, 0.72), 0.55 (0.35, 0.80) and 0.56 (0.38, 0.85) for CALITOO, the HHC and AERONET, respectively. The difference in the statistics for the three instruments at Lamto is due to different sampling periods (see Table 1), although the coincident observations between CALITOO and AERONET in 2017 show an excellent agreement (see below).

The median AE is between a minimum of 0.33 (0.13, 0.55) at Comé and a maximum of 0.78 (0.56, 1.09) at Koforidua. Observations performed with CALITOO at Lamto show a slightly lower range of AE values than the ones performed with the HHC. The difference between CALITOO median AE and HHC median AE is −0.09. However it should be noted that the statistical distribution of AOD values has an impact on the corresponding AE distribution (Wagner et al., 2008). AOD observed at Lamto during the HHC period (2006–2008) being higher than the ones observed during the CALITOO period (2014–2016), it is not expected to have the same AE values. Nonetheless, the difference is within the expected accuracy.

Coincident AERONET and CALITOO observations ($N = 31$) were acquired between January and March 2017 at Lamto (see Fig. 3 and Table 1). Figure 2 shows the scatterplot for the corresponding daily AOD and AE There is an excellent agreement for both AOD (regression coefficient $R = 0.93$) and AE ($R = 0.87$) between the two instruments.

3.2 Time series

The daily AODs and AEs for each site and each instrument between 2015 and 2017 (between 2006 and 2008 for HHC) are presented in Figs. 3 and 4, respectively. A similar seasonal pattern is observed in the different time series. There is an increase in AOD during the main dry season (December to March) and a decrease during the rainy season (April–July). The 2-week smoothing average reveals a high degree of correlation between time series. The correlation coefficient between Cotonou and Lamto time series is $R = 0.82$, with $R = 0.90$ between Cotonou and Koforidua. During the short overlap period in March 2017, the CALITOO and AERONET instruments show similar AOD values at Lamto station. The Comoé time series is the weakest one, with only 82 data points. The 2006–2008 HHC Lamto time series has the same pattern as the one recorded by CALITOO in 2015–2017 and shows two maxima in the dry season, one in December and another one in January–February.

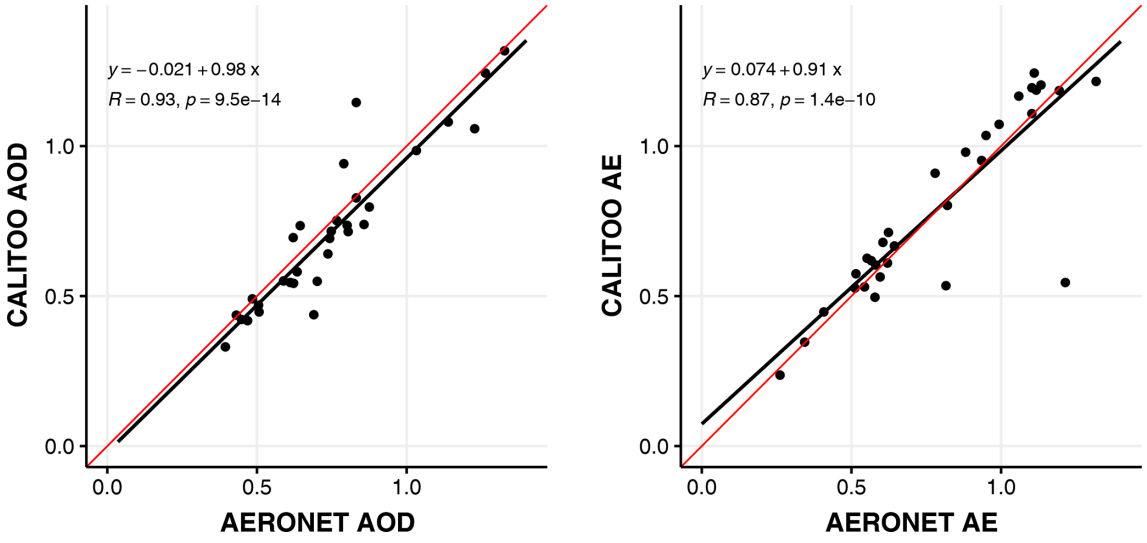

Figure 2. Scatterplot of AOD and AE observed at Lamto by the CALITOO and AERONET instruments between January and March 2017 (number of points = 31).

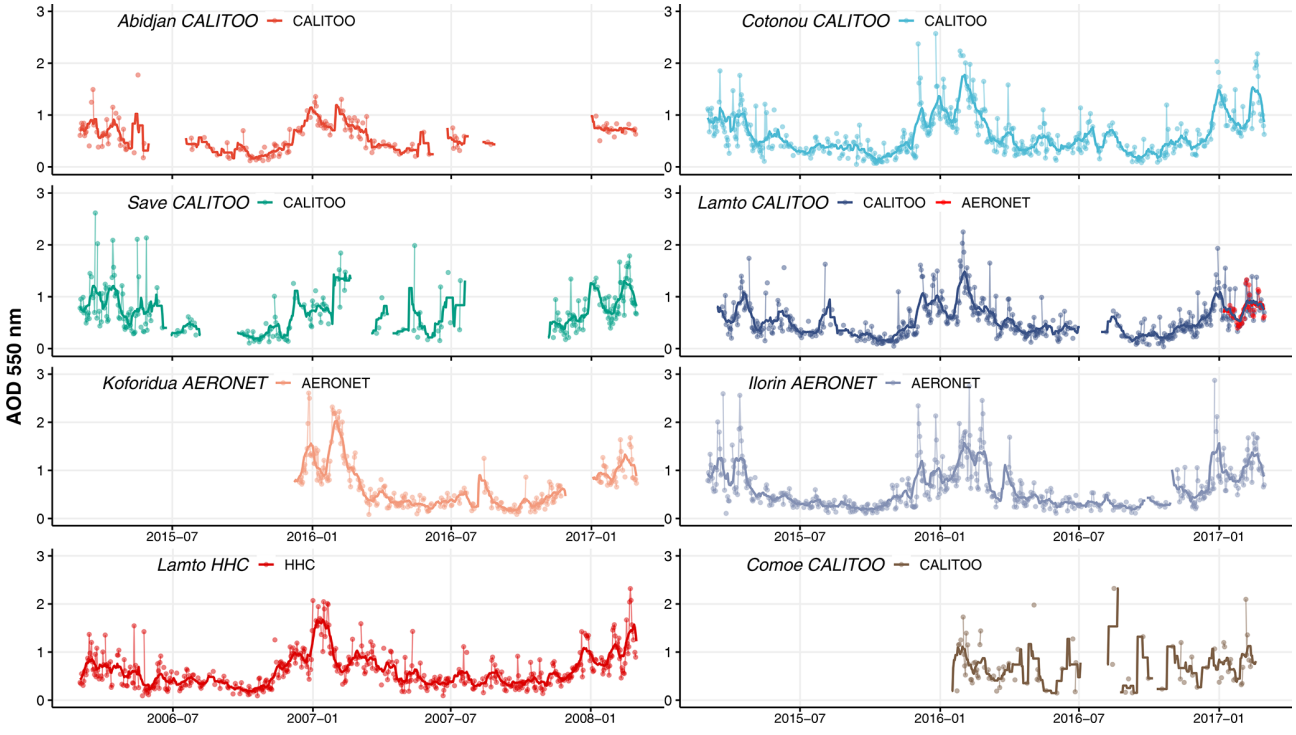

Figure 3. Daily aerosol optical depth at 550 nm. The name of the site and the type of instrument used are given in the legend of each plot. The solid line is a 2-week smoothing average.

The seasonal pattern for AEs (Fig. 4) shows an opposite cycle, with lower values in the dry season and higher values during the rainy season. AE seasonal cycle is clearly affected by the winter dry period, with dust-laden air masses that decrease the AE values. The median AE value during the first half of the year (all sites except Comoé) is 0.36 (0.23, 0.62) and 0.69 (0.43, 1.00) during the second half of the year. AODs in the last quartile (AOD above 0.82) are mostly (72 %) observed during the months of December, January and February and are associated with a median AE of 0.44 (0.24, 0.64), while low AODs (first quartile, i.e., below 0.33) are associated with a median AE of 0.89 (0.61, 1.12) and are observed between August and October (51 % of the observations). The difference in AOD between the inland and

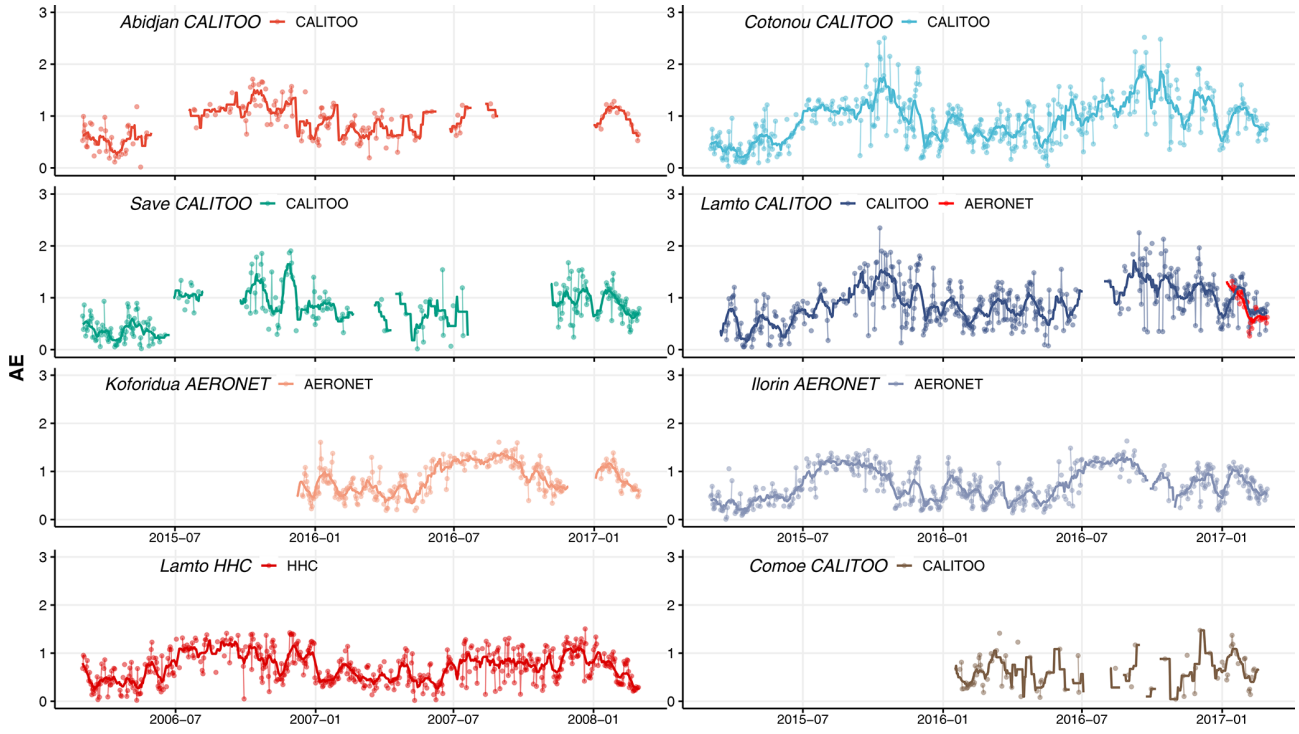

Figure 4. Same as Fig. 3 for the visible Ångström exponent.

the coastal sites is less than 0.05, with differences up to 0.1 between April and June, the AOD at the coastal stations being higher than inland. AEs are higher at the coastal stations than at the inland stations by 0.15 on average, reflecting the influence of urban air pollution at the coastal stations.

3.3 Comparison with MODIS aerosol products

Table 2 gives the statistics of the regressions for each site and per instrument presented in Fig. 5. We have then adopted a log–log representation on the scatterplots presented in Fig. 5 as the AOD distribution has a significant right skewness (O'Neill et al., 2000). Figure 5 also presents the MODIS expected error (EE; blue lines). Whatever the site is, there is a significant correlation between the MODIS and sun photometer observations. The Pearson correlation coefficient R ranges between 0.75 (Comoé) and 0.94 (Koforidua). For the CALITOO observations, R is between 0.75 and 0.90 (Cotonou). The lowest RMSE values are found for the measurements operated using the CALITOO at the coastal sites of Abidjan and Cotonou. The mean absolute percentage error (MAPE) is on average 30 %. The sites in Cotonou and Abdijan are not biased and present a fraction of data falling within the MODIS EE above 60 %. All the inland sites are biased, and it results in a rather low fraction of data falling within the MODIS expected error.

The bias has a seasonal behavior that is highest during the dry season, between December and March. An underestimation of the MODIS AOD is then observed at maximum in January, with an absolute bias of −0.33 (relative bias of 39 %) at the inland sites. Sayer et al. (2014) have already pointed out the possible differences in the "Dark Target" and "Deep Blue" algorithms. It appears from Fig. 6 in Sayer et al. (2014) that the dry-to-humid-savanna transition zone in SWA is an area where large differences exist in both retrieval techniques during the dry season. Those differences can explain that the "merge" product used in this study has a large bias during the dry season in the northern part for the inland sites, so the north–south AOD gradient in this area remains difficult to assess based on satellite products.

For all the sites considered in this study and whatever the sun photometer is, the correlation between MODIS AE and sun photometer AE is non-significant. This finding is coherent with the results of Antuña-Marrero et al. (2018) and Sayer et al. (2013). The histograms of the sun photometer and MODIS-derived AE are presented in Fig. 6. The default values AE = 1.5 and AE = 1.8 in the MODIS AE Deep Blue product have been removed (Sayer et al., 2013). The MODIS median AE is biased by 0.32, and the distribution of AE values does not follow a normal distribution, whereas the distribution of AE values for the sun photometers does. At the coastal sites, the MODIS AE Ocean algorithm reproduces well the left side of the histogram (lowest AE), while it significantly underestimates AE above 0.8. MODIS AE Land algorithm at 0.5 indicates that a dust-like aerosol model has been selected (Levy et al., 2010); however there is no systematic association with low sun photometer AE. However

Table 2. Results of the MODIS and sun photometer AOD comparison by site location and type of instrument, indicating the number of data (N), Pearson correlation coefficient (R), root mean square error (RMSE), bias, mean absolute percentage error (MAPE) and fraction falling within the MODIS expected error (fEE).

Site	Instrument	N	R	RMSE	Bias	MAPE	fEE
Cotonou	CALITOO	401	0.88	0.22	−0.02	24	64
Savè	CALITOO	254	0.79	0.31	−0.19	35	35
Abidjan	CALITOO	118	0.86	0.14	−0.02	18	76
Lamto	CALITOO	185	0.86	0.26	−0.15	29	50
Comoé	CALITOO	47	0.76	0.37	−0.22	32	44
Ilorin	AERONET	264	0.91	0.32	−0.19	33	39
Koforidua	AERONET	144	0.93	0.30	−0.20	26	46
Lamto	AERONET	17	0.87	0.34	−0.32	50	0
Lamto	HHC	181	0.83	0.39	−0.29	37	25

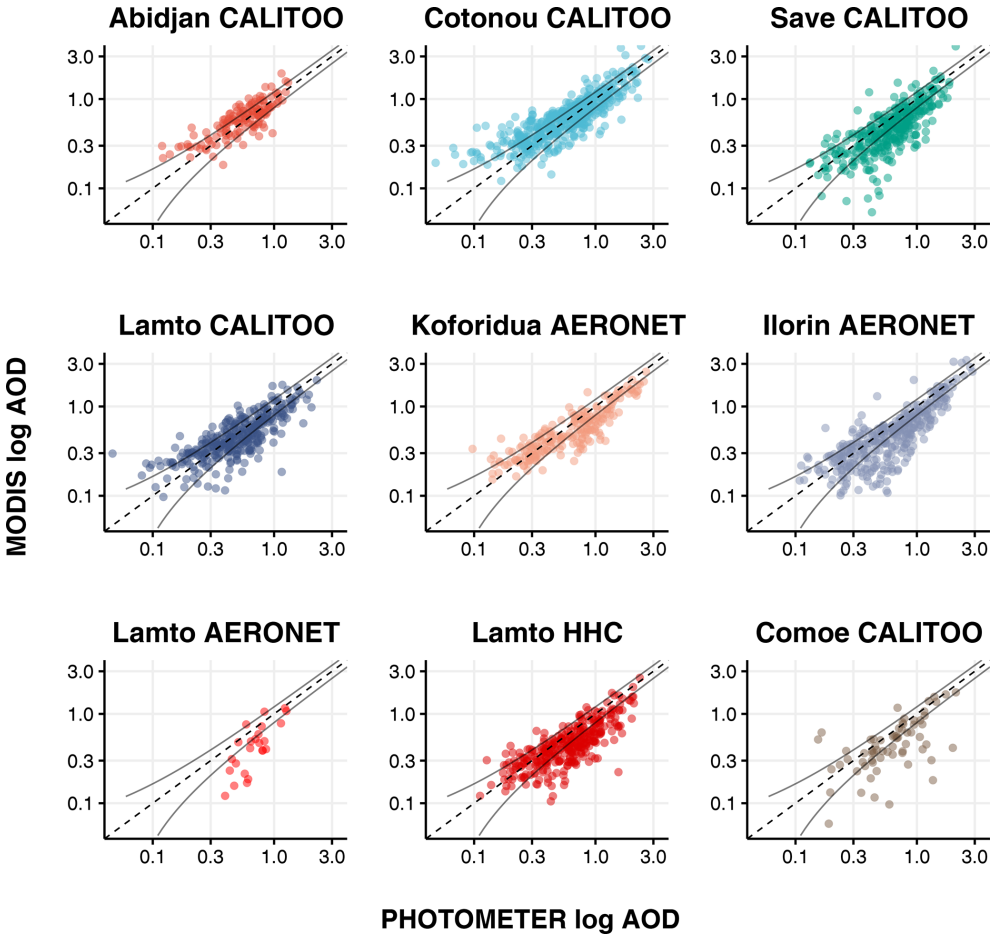

Figure 5. Scatterplots of MODIS vs. sun photometer AOD for the three types of sun photometers (automatic AERONET and handheld CALITOO and CIMEL) and different sites (Lamto, Comoé, Savè, Cotonou, Abidjan, Ilorin, Koforidua).

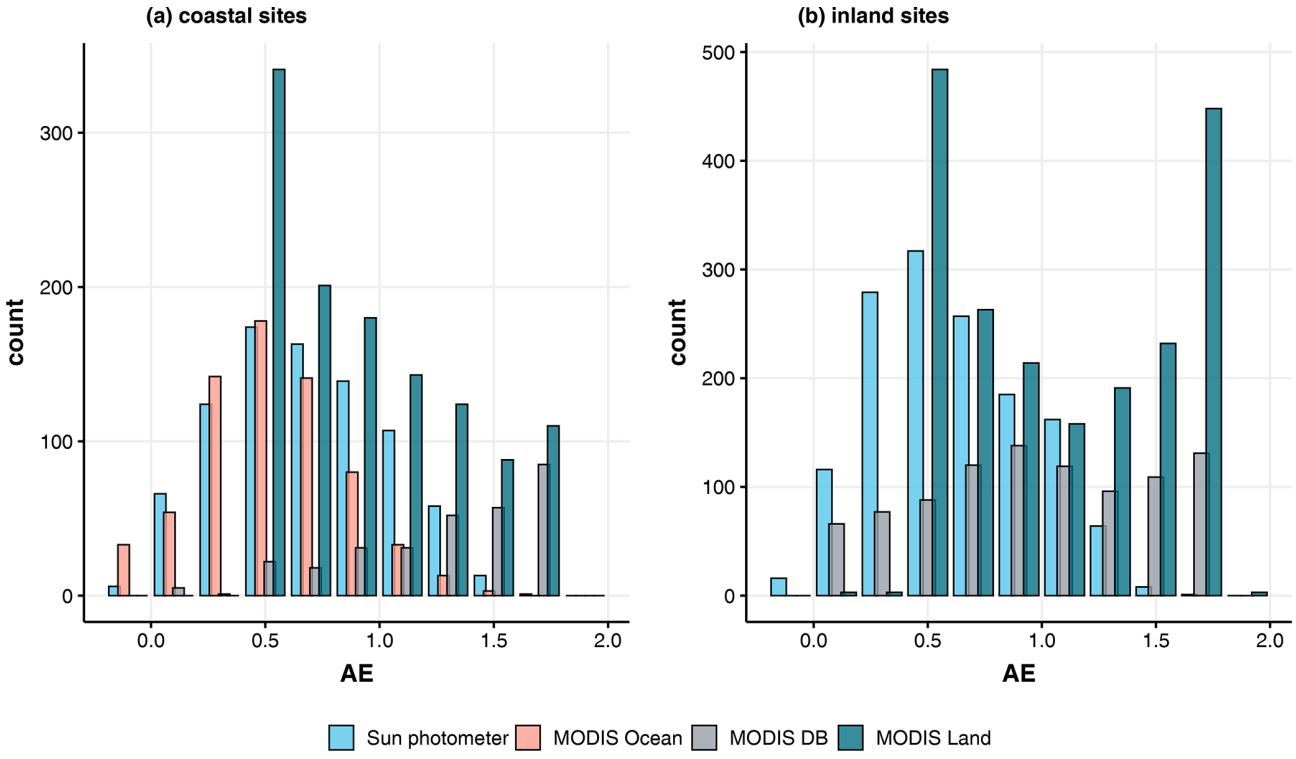

Figure 6. Comparative histograms of Ångström exponents for coincident sun photometer, MODIS Deep Blue, and MODIS Land and Ocean algorithms for **(a)** coastal sites and **(b)** inland sites.

it could be possible to adapt the interval bounds (lower and upper limits of AE values) for each category; the statistical distribution of MODIS AE values does not fit the sun photometer ones and could lead to misclassification of daily observations.

4 Aerosol type and relationship with surface concentrations

4.1 Aerosol type

AE is an intensive aerosol optical parameter and depends on the spectral aerosol extinction coefficient (Nakajima et al., 1996; Eck et al., 1999; Holben et al., 2001). AE is influenced by the aerosol size distribution and is commonly used to identify aerosol types (Léon et al., 1999; Kaskaoutis et al., 2009; Perrone et al., 2005). Aerosol types having a dominant fraction of their size distribution in the coarse mode, like dust and sea salt particles, are associated with a lower value of AE than aerosol types with a size distribution dominated by the accumulation mode, like secondary and combustion aerosols. The concurrent changes in AOD and AE help to distinguish generic aerosol types in sun photometer time series (Toledano et al., 2007; Verma, 2015). Mineral dust tends to increase atmospheric AOD and decrease AE (Hamonou et al., 1999), while biomass-burning events tend to increase both AE and AOD (Eck et al., 2003).

The AOD vs. AE scatterplot can be used to cluster the observations by aerosol broad categories corresponding to a main source, like coarse mineral dust of biomass-burning aerosols. The thresholding in AOD and AE for aerosol type identification varies from one site to another and also depends on the distance from aerosol sources upwind of the site (Verma, 2015; Benkhalifa et al., 2017). In particular, the classification based on AOD vs. AE values is incapable of determining aerosol absorption properties (Giles et al., 2012; Cazorla et al., 2013). Figure 7 presents the scatterplots of AODs (log-scale) vs. AEs for each site and split by seasons. We have considered four seasons corresponding to the long dry season (December–March), the long wet season (April–June), the short dry (August–September) and short wet season (October–November). For the sites with the most comprehensive data set over the different seasons (Lamto, Cotonou, Koforidua, Ilorin) the AOD vs. AE plots show a similar pattern, with AODs decreasing almost linearly as AE increases. The lowest AEs are observed during the long dry season and are associated with the largest AODs, indicating the presence of coarse mineral dust. The presence of dust can be also observed in the long wet season. During the short dry season, all the sites excepted Comoé show larger AEs and lower AODs than for the other seasons.

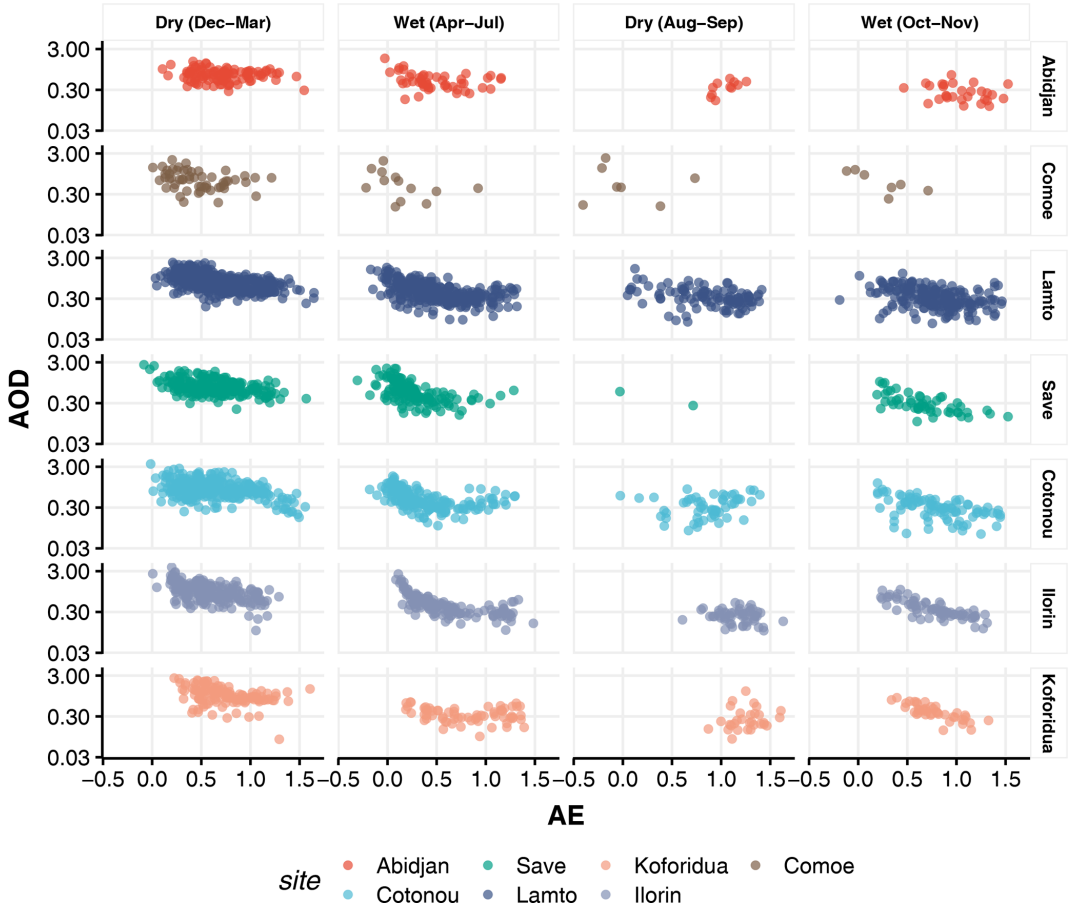

Figure 7. Scatterplots of sun photometer aerosol optical depth (AOD) vs. Ångström exponent (AE) split by sites and by seasons.

It can be noticed from Fig. 7 that there is no clear definition of AOD and AE thresholds for each aerosol category, and the scatterplots of Fig. 7 reflect the high mixing of different aerosol types. The absolute error in AE is a function of the relative error in AODs and depends on the spectral range investigated (Hamonou et al., 1999; Wagner et al., 2008). Typical error in AE is ± 0.3 for an AOD of 0.2, and there is a risk of overinterpreting AE variations.

In this paper we classify the daily observations according to the AE values using a simple statistical analysis and a threshold on AOD. The whole sun photometer data set is divided into three quantiles. The first third corresponds to AE ≤ 0.45, and observations having an AOD ≥ 0.8 are labeled "coarse dust", while observations having an AOD < 0.8 are labeled as "mixed". The threshold on AOD corresponds to the third quantile of AOD distribution and is used to better identify dust events. The last third corresponds to AE ≥ 0.80 and is labeled "urban-like". The data having $0.45 <$ AE < 0.80 fall into a "mixed" category, being more populated than the two others. This rather crude classification enables us to identify the main aerosol influence with a significant number of observations in each category.

Table 3. Percentage of daily observations in the aerosol categories at each site.

Site	Coarse dust	Mixed	Urban-like
Abidjan	3.7	56.8	39.5
Comoé	22.0	69.5	8.5
Lamto	8.6	56.5	34.9
Savè	12.2	67.9	20.0
Cotonou	10.2	57.6	32.2
Ilorin	12.7	50.6	36.7
Koforidua	4.9	47.3	47.7

Table 3 presents the typology of the sites according to the aforementioned classification. Comoé is the most influenced by coarse dust aerosol (20 %), followed by Ilorin (12.7 %), Savè (12.2 %), Cotonou (10.2 %) and Lamto (8.6 %). The southwestern sites, Abidjan (3.7 %) and Koforidua (4.9 %), are less influenced by dust events than the eastern sites. As expected from Fig. 7, all the sites show the "urban-like" category that also corresponds to low AODs. Two sites are less influenced by urban-like aerosols than the others, namely Savè (20 %) and Comoé (8.5 %). For the other sites, the

"urban-like" category ranges between 47.7 % (Koforidua) and 32.2 % (Cotonou).

As SWA lacks dedicated studies on aerosol characterization, there are few other data to compare with. Hamill et al. (2016) have proposed a sophisticated aerosol classification for Africa based on AERONET observations; however none of the sites are located in our area. Hamill et al. (2016) have classified Djougou (northern Benin, located at 9°42′ N) as a dust site that is seldom affected by biomass burning. Savè and Ilorin are located around 200 km south of Djougou, and the influence of dust is still significant compared to the coastal sites. Comoé is located 600 km westward of Djougou and probably less influenced by the dust transport from the Bodélé area in Chad; however measurements acquired at Comoé do not cover a full season, and the exact frequency of dust or biomass-burning events remains uncertain.

4.2 Relationship to surface concentrations

The changeover between the monsoon and the harmattan results in a change in the vertical distribution of aerosol layers and in the type of aerosols Djossou et al. (2018). The harmattan flow carries continental aerosols in the lowest part of the atmosphere during the dry winter season (December to March). During the dry winter season the days with high AOD are often associated with an increase in the $PM_{2.5}$ surface concentration, leading to a high correlation coefficient between AOD and $PM_{2.5.}$

The correlation coefficient between weekly mean AOD and $PM_{2.5}$ measured in Cotonou and Abidjan is $R = 0.75$ ($N = 105$) when considering the whole observation period. The correlation coefficient can reach $R = 0.96$ ($N = 6$) during specific aerosol events observed from December 2015 to January 2016 in the heart of the dry season. During other periods of the year, the correlation remains weak because the concentrations are less fluctuating than during the winter period.

$PM_{2.5}$/AOD ratios are estimated using the daily AOD observations and the weekly $PM_{2.5.}$ The $PM_{2.5}$/AOD is basically the amount of $PM_{2.5}$ that is expected per unit of AOD. It was first promoted by van Donkelaar et al. (2010) as a conversion factor (Zheng et al., 2017; Yang et al., 2019). The $PM_{2.5}$/AOD ratio reflects how a change in the AOD affects the ground surface concentrations; however there is no evidence of a unique relationship between both quantities. The $PM_{2.5}$/AOD ratio depends on the vertical stratification of the aerosol layers in the atmosphere due to mixing processes in the boundary layer or large-scale advection (Sayer et al., 2016). The ratio depends also on the aerosol size distribution and chemical properties that are changing during the transport and the aging of the aerosols.

In the specific case of the coastal cities of the Gulf of Guinea, we are interested in evaluating how the change in aerosol type during the season, and in particular the seasonal advection of mineral dust from the desert area, may affect the $PM_{2.5}$ surface concentrations. For this purpose, we estimate a $PM_{2.5}$/AOD ratio per aerosol type and per season.

Each daily AOD observation is associated with an aerosol type (coarse dust, mixed or urban-like) depending on the corresponding daily AE value. The daily AODs are associated with the corresponding $PM_{2.5}$ observation using Eq. (1).

$$PM_{2.5\text{weekly}} = \frac{1}{n}\sum_{i=1}^{n}\left(\sum_{t=1}^{3}\beta_{t,s}\,\tau_{i,t,s}\right) \quad (1)$$

The corresponding $PM_{2.5}$/AOD coefficients – $\beta_{t,s}$ in Eq. (1), where t represents the aerosol type and s the season – are evaluated using a multilinear regression on the observations collected in Cotonou and Abidjan for each season independently. Cotonou and Abidjan samples are pooled together to increase the statistical significance and to retrieve average coefficients at the regional level. As the season are not equal in length, and the number of observations differs in Abidjan and Cotonou, the number of samples differs, ranging between 71 samples during the long dry season and 24 samples during the short dry season. The significance of the regression and standard error in the coefficients depends on the number of samples. None of the weeks in the short dry period are affected by dusty days, so the coefficient for coarse dust is not retrieved for this period. During the short wet season, only 2 weeks over 26 have a dust contribution, and the coefficient is not significant. The $PM_{2.5}$/AOD ratios by aerosol category are presented in Fig. 8 as a function of the season and with their respective uncertainties. The average $PM_{2.5}$/AOD ratio without accounting for the aerosol category for a given season is also reported. The uncertainties correspond to the standard error in the coefficients found by regression. The standard error depends on the occurrence of an aerosol category and its relative weight in a given season. For all the seasons the coefficients for each aerosol type are significant ($p < 0.05$), except for the coarse dust category during the short dry (no data) and the short wet season. The resulting adjusted coefficient of determination for the regression is between 0.76 (long dry season) and 0.83 (short wet season).

The $PM_{2.5}$/AOD ratio for coarse dust aerosols ranges between $54 \pm 8\,\mu g\,m^{-3}$ per unit AOD in the long dry season and $20 \pm 4\,\mu g\,m^{-3}$ per unit AOD in the long wet season. The seasonal changes in the $PM_{2.5}$/AOD ratio for coarse dust reflects well the vertical shift in the dust layer between the dry and the wet season. During the wet (April–July) season, the air masses are uplifted by the monsoon flow. $PM_{2.5}$ concentrations remain moderate ($21\,\mu g\,m^{-3}$ in April), while AODs are still significant (0.57 on average in April) due to the aloft transport. The impact of coarse dust on $PM_{2.5}$ is higher during the dry season (higher ratio and high AODs), when the dusty air masses are advected close to the ground surface.

The $PM_{2.5}$/AOD ratio for mixed aerosols ranges between $53 \pm 7\,\mu g\,m^{-3}$ per unit AOD in the long dry season and $27 \pm 11\,\mu g\,m^{-3}$ per unit AOD in the short dry season. During the short dry season, only 30 % of the weeks are affected by

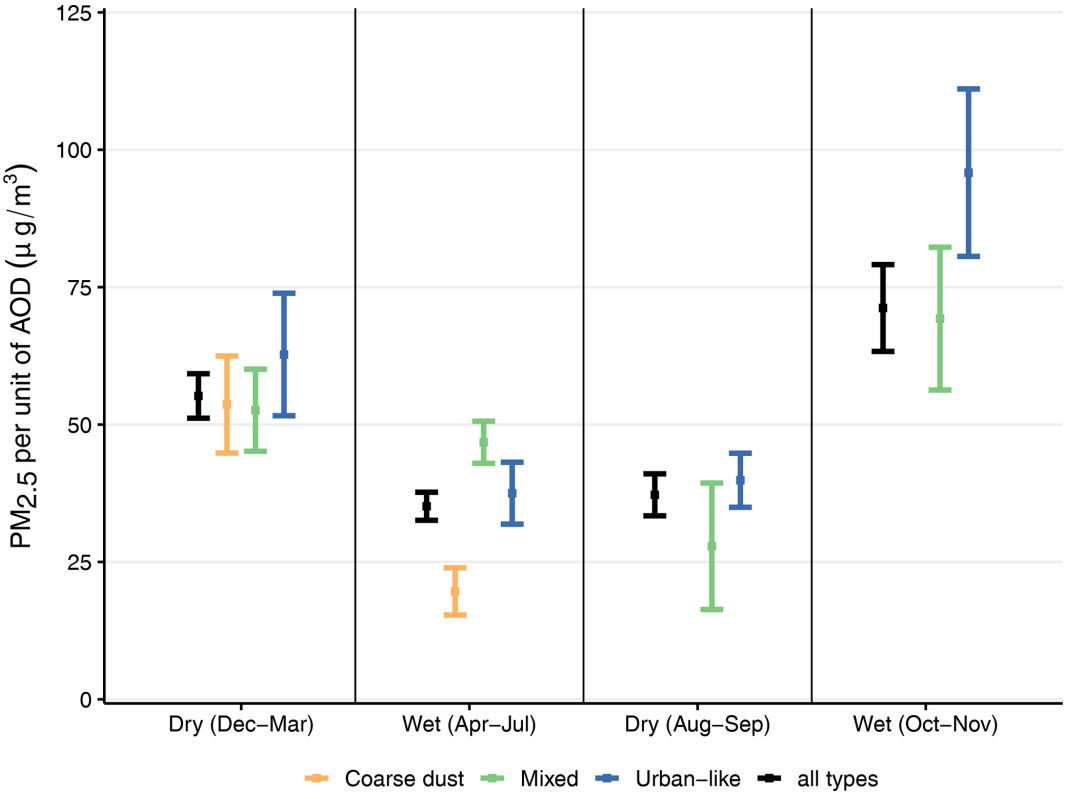

Figure 8. Ratio of $PM_{2.5}$ to AOD for each of the aerosol types during the long dry (December–March) and long wet (April–June) seasons and the short dry (August–September) and short wet (October–November) seasons. Data are collected in Abidjan and Cotonou from 2015 to 2017.

mixed-type aerosols, the remaining being classified as urban-like. The corresponding $PM_{2.5}$/AOD ratio for mixed-type aerosol is close to the one found for dust during the previous season (long wet), indicating that the aloft dust transport can be still active but incorrectly classified to the mixed aerosol type due to a low intensity (small AOD).

The $PM_{2.5}$/AOD ratio for urban-like aerosols ranges between $96 \pm 15\,\mu g\,m^{-3}$ per unit AOD in the short wet season and $37 \pm 5\,\mu g\,m^{-3}$ per unit AOD in the long wet season. The $PM_{2.5}$/AOD ratio retrieved in the long dry season for the urban-like category is affected by a larger uncertainty due to a limited impact of urban-like aerosol during the long dry season compared to coarse dust. There is a shift in the $PM_{2.5}$/AOD ratio toward higher values during the short wet season. The short wet season is a transition period during which the stagnation of air masses over land favors the accumulation of pollutants and also combustion by-products emitted over Nigeria (Marais et al., 2014).

Figure 9 presents the weekly average AODs and satellite-derived and in situ $PM_{2.5}$ for both Abidjan and Cotonou. The label attributed to each week corresponds to the aerosol type having the largest mean AOD over the week. The period from March to May is dominated by the coarse dust type, and there is a clear shift to urban-like type in June–July. A second period of coarse dust is observed in December (2015 and 2016) and is associated with a significant increase in both AOD and $PM_{2.5}$. $PM_{2.5}$ during the dusty period of December rises over $100\,\mu g\,m^{-3}$. Another sharp increase is observed in February and is associated with the mixed aerosol type. For both years, the two intense periods (December and February) are separated by an interim period showing moderate $PM_{2.5}$ and AOD and classified as urban-like aerosols.

On average, satellite-derived $PM_{2.5}$ agrees with the in situ $PM_{2.5}$ observations. Indeed the mean difference between retrieved and observed $PM_{2.5}$ during the 2015–2016 period is less than $1\,\mu g\,m^{-3}$ (3 %). The MAE is $14\,\mu g\,m^{-3}$, and the RMSE is $21\,\mu g\,m^{-3}$. The RMSE found here is within the range of previous studies (Ma et al., 2015; Sinha et al., 2015) for other regions of the world and different algorithms. The very intense periods are underestimated; e.g., the mean difference between retrieved and observed $PM_{2.5}$ is $-51\,\mu g\,m^{-3}$ (-70 %) in December 2015 in Cotonou and nearly a factor of 2 lower in December 2016. The satellite-derived concentrations in January and in March are overestimated. Despite introducing a characterization of the aerosol type, there is still a clear smoothing effect on the weekly concentrations that results from the adjustment of the regression coefficients on a seasonal basis. Using seasonally adjusted coefficients

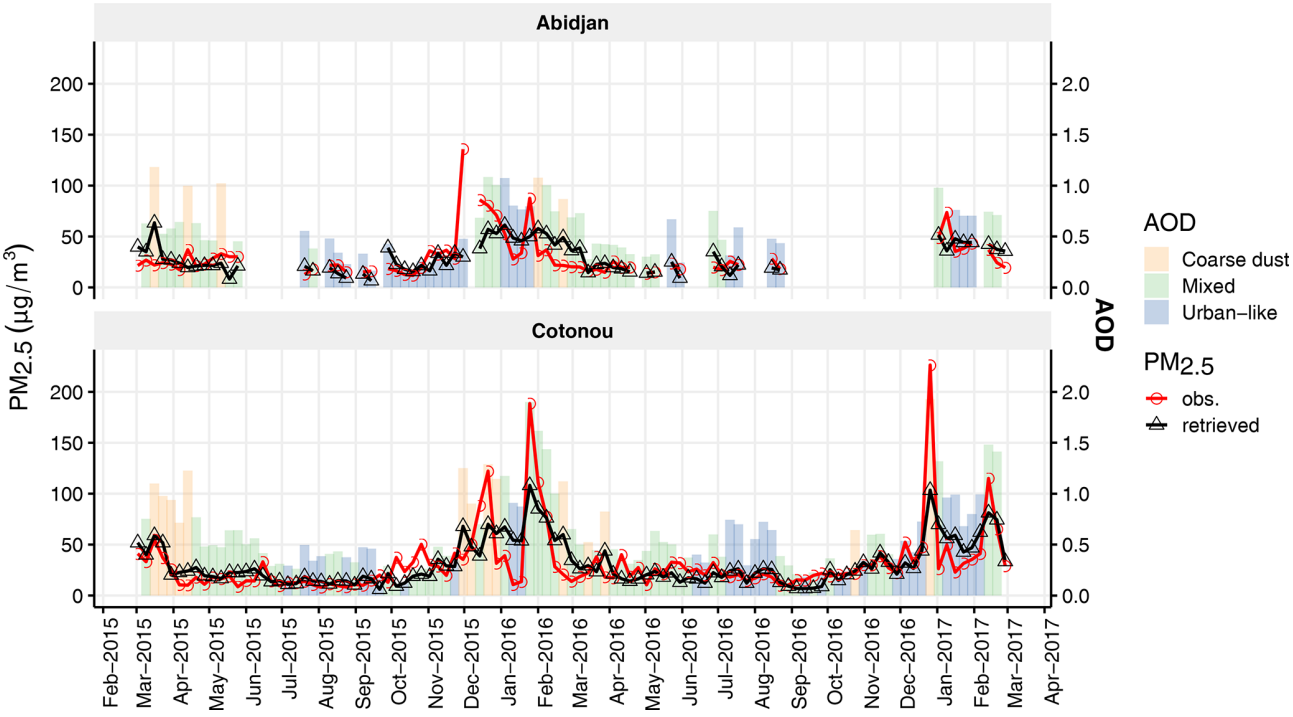

Figure 9. In situ and AOD-derived mean weekly $PM_{2.5}$ from March 2015 to March 2017 in Abidjan and Cotonou. Vertical color bars give the weekly AOD by aerosol category.

only rather than the seasonally adjusted and aerosol-type-adjusted coefficients has a limited impact on the comparison and decreases the RMSE by only $2\,\mu g\,m^{-3}$ on average. The biggest impact is during the long wet season (20 % decrease in RMSE), when a lower $PM_{2.5}$/AOD coefficient is selected for the identified dust cases.

5 Trend in the MODIS-derived $PM_{2.5}$ time series

We have applied the $PM_{2.5}$-to-AOD conversion factors to the daily MODIS AOD observations between 2003 and 2019. As the MODIS AE cannot be used to classified the daily aerosol observations, we have applied the mean seasonaly adjusted $PM_{2.5}$/AOD ratios. The database of daily AOD observations consists of 2675 observations for the area of Abidjan and 3018 for the area of Cotonou, corresponding to about 160 observations per year on average. To increase the number of observations per year, we introduce a new area named SWA, located between 7° W and 5° E and between 6° N and 4° N. There is at least one MODIS level 3 observation per day in the largest coastal area that encompasses both cities.

Mean retrieved $PM_{2.5}$ is 28.3 ± 22.2 and $30.5 \pm 24\,\mu g\,m^{-3}$ in Abidjan and Cotonou, respectively. Almost all the years have an annual average above the EU target value of $25\,\mu g\,m^{-3}$, except 2003, 2013, 2014 and 2019. More than 90 % of the daily observations are above $10\,\mu g\,m^{-3}$ for both cities. A maximum is observed as high as $300\,\mu g\,m^{-3}$ during dust event in winter 2010 in Abidjan. During the long dry season 80 % of the days have a value above $35\,\mu g\,m^{-3}$, while this number drops to 4 % during the short dry season.

The MODIS-derived $PM_{2.5}$ monthly mean annual cycle given in Fig. 10 for both cities and the SWA area reflects this large seasonal change in the concentrations. A first period is observed between December and March, when concentrations are the highest. During this period, the overall mean $PM_{2.5}$ value is $47\,\mu g\,m^{-3}$, concentrations in Cotonou being higher than in Abidjan (max. 11 % in January). We observe a large difference in April (18 % higher in Cotonou) that is clearly attributed to a change in the contribution of coarse dust (+34 % in Cotonou), while the contribution of other types remains the same. This higher contribution of dust during the dry period and even more during the intermediate period over Cotonou could be associated with the higher proximity of Cotonou to major dust sources (Bodélé depression) and preferential advection pathways.

A second period is observed between May and September showing mean $PM_{2.5}$ below $16\,\mu g\,m^{-3}$ for both cities and the whole area. The third period corresponds to a steady increase in $PM_{2.5}$ between September and December. $PM_{2.5}$ mean concentration over the SWA area is around $11\,\mu g\,m^{-3}$ in September and increases up to $37\,\mu g\,m^{-3}$ in December, corresponding to an increase by a factor of about 3 in 4 months. A similar increase is observed for Abidjan and Cotonou.

The monthly mean $PM_{2.5}$ displayed in Fig. 11a shows the strong seasonal variation with the highest values in Jan-

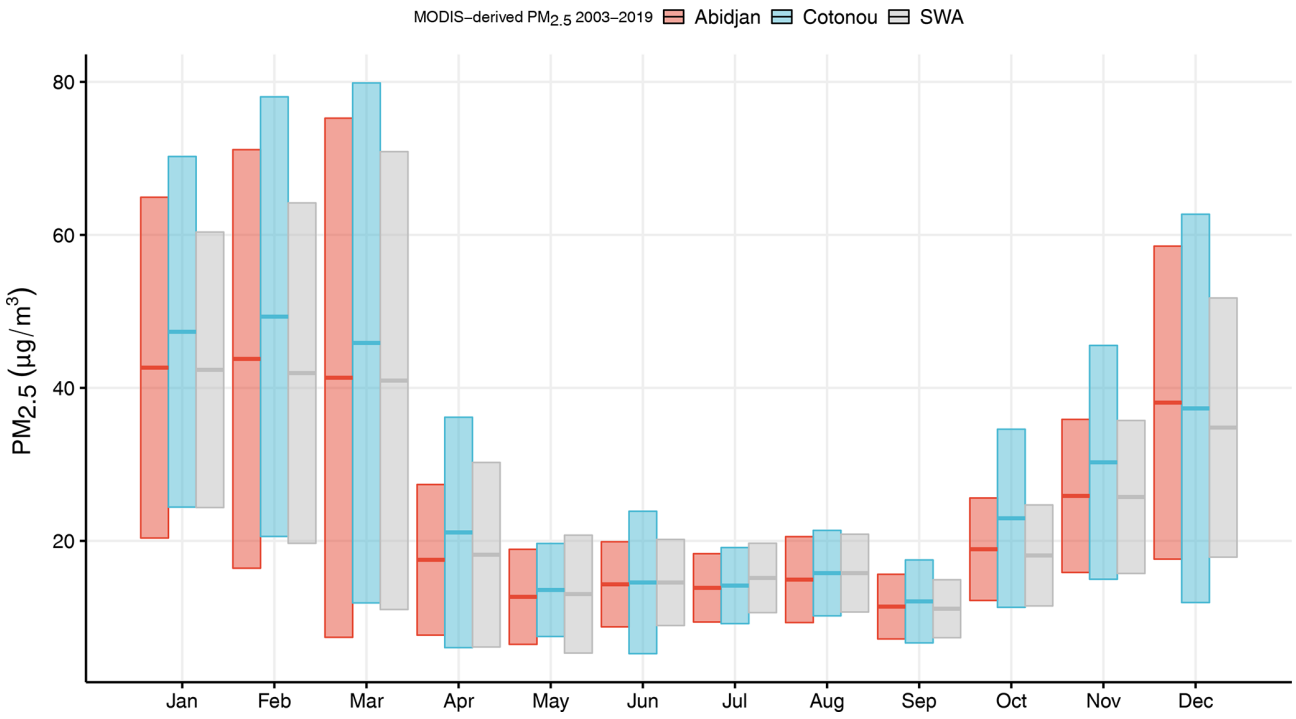

Figure 10. Monthly mean annual cycle of MODIS-derived $PM_{2.5}$ in Abidjan and Cotonou and the SWA area between 2003 and 2019. Boxes represents the mean ± 1 standard deviation.

uary or February every year. The trend of monthly means is retrieved after a seasonal decomposition using a procedure based on loess (Cleveland et al., 1990). The trend does not have an obvious pattern; however one can observe a pseudo-cycle of 4 to 5 years. We can notice a decrease in the mean concentrations after 2017. The drop in 2018 and 2019 is due to lower AODs for those 2 years. The annual mean AOD decreases by 20 % between 2017 and 2019; however we did not investigated further a possible explanation for the decrease. The Mann–Kendall seasonal trend test (Hirsch et al., 1982) applied to monthly means is not significant over the whole 2003–2019 period.

To further investigate a possible trend in the urban-like aerosol, we have selected the data acquired during the short dry period (August–September), during which no dust events have been detected in our sun photometer data set. Over the period 2003–2017, we observe a monotonic trend (Mann–Kendall's tau = 0.48) in the annual mean MODIS-derived $PM_{2.5}$ over the SWA box (Fig. 11b). The Thiel–Sen slope over 2003–2017 is 0.20 with a 95 % confidence interval of [0.04, 0.43], corresponding to a monotonic increase in $PM_{2.5}$ of $3.0\,\mu g\,m^{-3}$ over 15 years. The large uncertainty in the observed trend during the short dry period is due to the low $PM_{2.5}$ concentrations observed during this period (see Fig. 10). As $PM_{2.5}$ is directly linked to AOD, any bias occurring in AOD will affect the $PM_{2.5}$ concentrations. Moreover the drift in the MODIS AQUA calibration expressed in AOD per decade is 0.01 (Sayer et al., 2019) and will lead to an increase of the same order of magnitude when considering the corresponding $PM_{2.5}$-to-AOD conversion coefficient.

6 Conclusions

An increase in the anthropogenic emission of atmospheric pollutants is expected as a result of the massive urbanization of the Gulf of Guinea. The scarcity of ground-based observations in SWA is still a limiting factor for a comprehensive understanding of the short-time trend over growing African cities. Moreover, the large influence of natural aerosol emission in SWA produces a complex mixing of particles in the urban atmosphere of SWA cities. In this paper, sun photometer and satellite observations have been used to characterize the magnitude and seasonal behavior of the aerosol optical depth in SWA. We have set up a small network of lightweight handheld sun photometers that provides an unprecedented data set on the AOD over SWA between 2015 and 2017. This data set was complemented by additional measurements from AERONET data and observations obtained during a previous campaign in 2006 in Côte d'Ivoire. The comparison of our observations with the MODIS level 3 gridded satellite observations shows that the satellite AOD derived in the vicinity of the coastal conurbation is excellent, while there is a possible negative bias for the retrievals farther inland that must be further investigated. Reversely the MODIS AE does not fit the sun photometer observations.

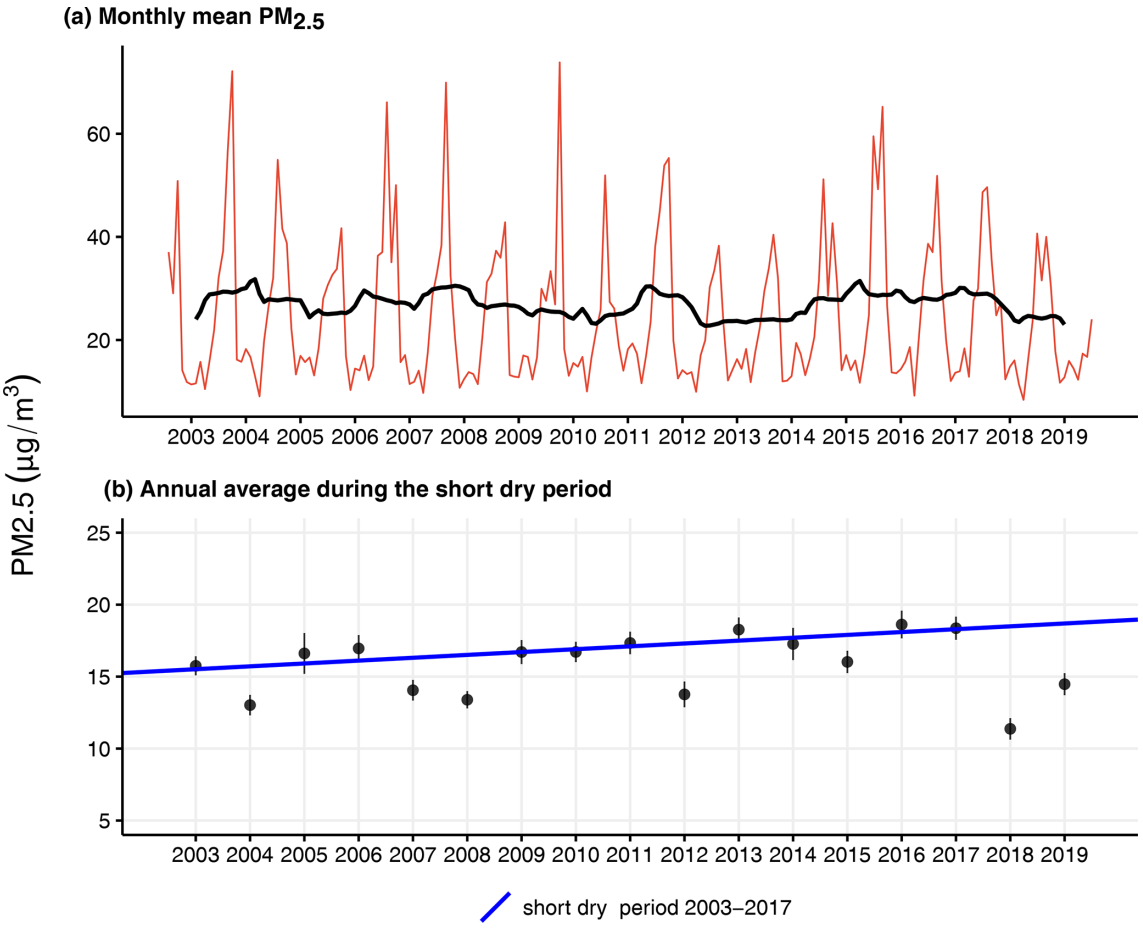

Figure 11. MODIS-derived $PM_{2.5}$ from 2003 to 2019. **(a)** Monthly mean over SWA and seasonal adjusted trend, **(b)** annual average during the short dry period and monotonic trend computed over 2003–2017.

A basic classification using the AOD spectral dependency reveals the large impact of the advection of mineral dust on the AOD seasonal cycle. Dust impacts the cities of the northern part of the Gulf of Guinea (namely Abidjan and Cotonou in the present study) from December to May and brings the largest AODs during the months of December and February.

Weekly surface $PM_{2.5}$ in Abidjan and Cotonou and daily AOD observations were used to estimate a set of AOD-to-$PM_{2.5}$ conversion coefficients that account for the aerosol category and the season. Despite a good agreement for most of the year, the retrieved $PM_{2.5}$ underestimates the actual concentrations during the large aerosol events in the dry season. Reversely the $PM_{2.5}$ is overestimated in early March as a consequence of the shift in altitude of the Harmattan wind. Nonetheless the seasonal variability in the $PM_{2.5}$ concentrations is in good agreement with the actual ones.

The seasonal $PM_{2.5}$-to-AOD conversion coefficients are applied to the MODIS AOD time series from 2003 to 2019. It was not possible to adjust the $PM_{2.5}$/AOD ratio both seasonally and by aerosol type due to the lack of precision in the MODIS AE. No obvious trend is observed in the mean monthly concentrations; however the trend fluctuates with a pseudo-period of 4 to 5 years. A link to the 5-year cycle of rainfall in the Sahel (Brandt et al., 2019) could be involved as rainfall is one of the main drivers of dust emission (Prospero and Nees, 1977) and also as it controls the amount of biomass that can be burned.

An increase in MODIS-derived $PM_{2.5}$ is observed over the 2003–2017 period during the short dry period (August–September). The trend corresponds to an increase of 20 % over 15 years. There are several mechanisms that can lead to the increase in the anthropogenic $PM_{2.5}$ concentrations. Combustion sources are subject to an increase in SWA as well as for the rest of Africa; e.g., organic-carbon emissions are multiplied by a factor of between 1.5 and 3.0 over 2005–2030 (Liousse et al., 2014). The conurbations of the Gulf of Guinea are under the influence of gas flaring emissions in the Niger Delta area (Ologunorisa, 2001). Recent studies show a decrease in gas flaring emissions in the Niger Delta area (Deetz and Vogel, 2017; Doumbia et al., 2019), but the impact of the year-to-year variability in such emissions on regional atmospheric concentrations has to be further inves-

tigated. The increase found during the short dry period corresponds to an average annual growth rate of 1.1 %, which is in the lower bound of the emission scenario; however there is no evidence that the observed trend is directly linked to an increase in the urban emissions. The phenomena can also be linked to the possible advection of biomass-burning by-products from central Africa and crossing the Gulf of Guinea, resulting from the zonal transport (Menut et al., 2018; Flamant et al., 2018).

While SWA has received little attention regarding anthropogenic urban emissions, our study reports new observations and original analysis. Additional ground truths and advanced satellite aerosol products or a combination of products targeting aerosol attribution are required to unravel the relative impact of anthropogenic vs. natural aerosol emissions on atmospheric concentrations in this area of the world that is under growing anthropogenic pressure.

Data availability. Handheld sun photometer and $PM_{2.5}$ data are available at http://baobab.sedoo.fr/ (last access: 5 February 2021). AERONET sun photometer data are available at https://aeronet.gsfc.nasa.gov/ (last access: 5 February 2021). MODIS aerosol data can be downloaded from https://ladsweb.modaps.eosdis.nasa.gov/ (last access: 5 February 2021)

Author contributions. JFL, CL, ABA and VY designed the research and organized the field experiment. MoB, JD and MaB carried out the measurements and the analysis. JFL finalized the analysis and prepared the manuscript with contributions from all co-authors.

Competing interests. The authors declare that they have no conflict of interest.

Special issue statement. This article is part of the special issue "Results of the project "Dynamics-aerosol-chemistry-cloud interactions in West Africa" (DACCIWA) (ACP/AMT inter-journal SI)". It does not belong to a conference.

Acknowledgements. The authors greatly thank all the operators who contributed to the acquisition of handheld-sun-photometer observations at the Lamto geophysical station, CEG Dantokpa and CEG Savè. We acknowledge the AERONET and PHOTONS sun-photometer networks, their staff, and the PI of the sites for their work to produce the data set used in this study (http://aeronet.gsfc.nasa.gov/, last access: 5 February 2021). Handheld CIMEL data were processed by Isabelle Jankowiak (Laboratoire d'Optique Atmosphérique, Université Lille 1).

Financial support. This research has been supported by the FP7 Environment (DACCIWA; grant no. 603502).

Review statement. This paper was edited by Evangelos Gerasopoulos and reviewed by two anonymous referees.

References

Adetunji, J., McGregor, J., and Ong, C. K.: Harmattan Haze, Weather, 34, 430–436, https://doi.org/10.1002/j.1477-8696.1979.tb03389.x, 1979.

Adon, M., Galy-Lacaux, C., Yoboué, V., Delon, C., Lacaux, J. P., Castera, P., Gardrat, E., Pienaar, J., Al Ourabi, H., Laouali, D., Diop, B., Sigha-Nkamdjou, L., Akpo, A., Tathy, J. P., Lavenu, F., and Mougin, E.: Long term measurements of sulfur dioxide, nitrogen dioxide, ammonia, nitric acid and ozone in Africa using passive samplers, Atmos. Chem. Phys., 10, 7467–7487, https://doi.org/10.5194/acp-10-7467-2010, 2010.

Ångström, A.: Techniques of Determinig the Turbidity of the Atmosphere, Tellus, 13, 214–223, https://doi.org/10.1111/j.2153-3490.1961.tb00078.x, 1961.

AntuÑa-Marrero, J. C., Cachorro Revilla, V., García Parrado, F., de Frutos Baraja, Á., Rodríguez Vega, A., Mateos, D., Estevan Arredondo, R., and Toledano, C.: Comparison of aerosol optical depth from satellite (MODIS), sun photometer and broadband pyrheliometer ground-based observations in Cuba, Atmos. Meas. Tech., 11, 2279–2293, https://doi.org/10.5194/amt-11-2279-2018, 2018.

Basart, S., Pérez, C., Cuevas, E., Baldasano, J. M., and Gobbi, G. P.: Aerosol characterization in Northern Africa, Northeastern Atlantic, Mediterranean Basin and Middle East from direct-sun AERONET observations, Atmos. Chem. Phys., 9, 8265–8282, https://doi.org/10.5194/acp-9-8265-2009, 2009.

Benedetti, A., Morcrette, J.-J., Boucher, O., Dethof, A., Engelen, R. J., Fisher, M., Flentje, H., Huneeus, N., Jones, L., Kaiser, J. W., Kinne, S., Mangold, A., Razinger, M., Simmons, A. J., and Suttie, M.: Aerosol Analysis and Forecast in the European Centre for Medium-Range Weather Forecasts Integrated Forecast System: 2. Data Assimilation, J. Geophys. Res., 114, DS13205, https://doi.org/10.1029/2008JD011115, 2009.

Benkhalifa, J., Léon, J. F., and Chaabane, M.: Aerosol Optical Properties of Western Mediterranean Basin from Multi-Year AERONET Data, J. Atmos. Sol.-Terr. Phy., 164, 222–228, https://doi.org/10.1016/j.jastp.2017.08.029, 2017.

Boers, R., van Weele, M., van Meijgaard, E., Savenije, M., Siebesma, A. P., Bosveld, F., and Stammes, P.: Observations and Projections of Visibility and Aerosol Optical Thickness (1956–2100) in the Netherlands: Impacts of Time-Varying Aerosol Composition and Hygroscopicity, Environ. Res. Lett., 10, 015003, https://doi.org/10.1088/1748-9326/10/1/015003, 2015.

Boucher, O., Randall, D., Artaxo, P., Bretherton, C., Feingold, G., Forster, P., Kerminen, V.-M., Kondo, Y., Liao, H., Lohmann, U., Rasch, P., Satheesh, S. K., Sherwood, S. C., Stevens, B., and Zhang, X.: Clouds and Aerosols, in: Climate Change 2013: The Physical Science Basis. Contribution of Working Group I to the Fifth Assessment Report of the Intergovernmental Panel on Climate Change, Cambridge University Press, Cambridge, United Kingdom and New York, NY, USA, 571–657, 2013.

Boyouk, N., Léon, J. F., Delbarre, H., Podvin, T., and Deroo, C.: Impact of the Mixing Boundary Layer on the Relationship between

PM2.5 and Aerosol Optical Thickness, Atmos. Environ., 44, 271–277, https://doi.org/10.1016/j.atmosenv.2009.06.053, 2010.

Brandt, M., Hiernaux, P., Rasmussen, K., Tucker, C. J., Wigneron, J.-P., Diouf, A. A., Herrmann, S. M., Zhang, W., Kergoat, L., Mbow, C., Abel, C., Auda, Y., and Fensholt, R.: Changes in Rainfall Distribution Promote Woody Foliage Production in the Sahel, Commun. Biol., 2, 133, https://doi.org/10.1038/s42003-019-0383-9, 2019.

Cazorla, A., Bahadur, R., Suski, K. J., Cahill, J. F., Chand, D., Schmid, B., Ramanathan, V., and Prather, K. A.: Relating aerosol absorption due to soot, organic carbon, and dust to emission sources determined from in-situ chemical measurements, Atmos. Chem. Phys., 13, 9337–9350, https://doi.org/10.5194/acp-13-9337-2013, 2013.

Cleveland, R. B., Cleveland, W. S., McRae, J. E., and Terpenning, I.: STL: A Seasonal-Trend Decomposition Procedure Based on Loess (with Discussion), J. Off. Stat., 6, 3–73, 1990.

Deetz, K. and Vogel, B.: Development of a new gas-flaring emission dataset for southern West Africa, Geosci. Model Dev., 10, 1607–1620, https://doi.org/10.5194/gmd-10-1607-2017, 2017.

Djossou, J., Léon, J.-F., Akpo, A. B., Liousse, C., Yoboué, V., Bedou, M., Bodjrenou, M., Chiron, C., Galy-Lacaux, C., Gardrat, E., Abbey, M., Keita, S., Bahino, J., Touré N'Datchoh, E., Ossohou, M., and Awanou, C. N.: Mass concentration, optical depth and carbon composition of particulate matter in the major southern West African cities of Cotonou (Benin) and Abidjan (Côte d'Ivoire), Atmos. Chem. Phys., 18, 6275–6291, https://doi.org/10.5194/acp-18-6275-2018, 2018.

Doumbia, E. H. T., Liousse, C., Keita, S., Granier, L., Granier, C., Elvidge, C. D., Elguindi, N., and Law, K.: Flaring Emissions in Africa: Distribution, Evolution and Comparison with Current Inventories, Atmos. Environ., 199, 423–434, https://doi.org/10.1016/j.atmosenv.2018.11.006, 2019.

Eck, T. F., Holben, B. N., Reid, J. S., Dubovik, O., Smirnov, A., O'Neill, N. T., Slutsker, I., and Kinne, S.: Wavelength Dependence of the Optical Depth of Biomass Burning, Urban, and Desert Dust Aerosols, J. Geophys. Res., 104, 31333, https://doi.org/10.1029/1999JD900923, 1999.

Eck, T. F., Holben, B. N., Ward, D. E., Mukelabai, M. M., Dubovik, O., Smirnov, A., Schafer, J. S., Hsu, N. C., Piketh, S. J., Queface, A., Roux, J. L., Swap, R. J., and Slutsker, I.: Variability of Biomass Burning Aerosol Optical Characteristics in Southern Africa during the SAFARI 2000 Dry Season Campaign and a Comparison of Single Scattering Albedo Estimates from Radiometric Measurements, J. Geophys. Res.-Atmos., 108, 8477, https://doi.org/10.1029/2002JD002321, 2003.

Flamant, C., Deroubaix, A., Chazette, P., Brito, J., Gaetani, M., Knippertz, P., Fink, A. H., de Coetlogon, G., Menut, L., Colomb, A., Denjean, C., Meynadier, R., Rosenberg, P., Dupuy, R., Dominutti, P., Duplissy, J., Bourrianne, T., Schwarzenboeck, A., Ramonet, M., and Totems, J.: Aerosol distribution in the northern Gulf of Guinea: local anthropogenic sources, long-range transport, and the role of coastal shallow circulations, Atmos. Chem. Phys., 18, 12363–12389, https://doi.org/10.5194/acp-18-12363-2018, 2018.

Giles, D. M., Holben, B. N., Eck, T. F., Sinyuk, A., Smirnov, A., Slutsker, I., Dickerson, R. R., Thompson, A. M., and Schafer, J. S.: An Analysis of AERONET Aerosol Absorption Properties and Classifications Representative of Aerosol Source Regions, J. Geophys. Res.-Atmos., 117, D17203, https://doi.org/10.1029/2012JD018127, 2012.

Giles, D. M., Sinyuk, A., Sorokin, M. G., Schafer, J. S., Smirnov, A., Slutsker, I., Eck, T. F., Holben, B. N., Lewis, J. R., Campbell, J. R., Welton, E. J., Korkin, S. V., and Lyapustin, A. I.: Advancements in the Aerosol Robotic Network (AERONET) Version 3 database – automated near-real-time quality control algorithm with improved cloud screening for Sun photometer aerosol optical depth (AOD) measurements, Atmos. Meas. Tech., 12, 169–209, https://doi.org/10.5194/amt-12-169-2019, 2019.

Gupta, P. and Christopher, S. A.: Particulate Matter Air Quality Assessment Using Integrated Surface, Satellite, and Meteorological Products: Multiple Regression Approach, J. Geophys. Res., 114, D14205, https://doi.org/10.1029/2008JD011496, 2009.

Hamill, P., Giordano, M., Ward, C., Giles, D., and Holben, B.: An AERONET-Based Aerosol Classification Using the Mahalanobis Distance, Atmos. Environ., 140, 213–233, https://doi.org/10.1016/j.atmosenv.2016.06.002, 2016.

Hamonou, E., Chazette, P., Balis, D., Dulac, F., Schneider, X., Galani, E., Ancellet, G., and Papayannis, A.: Characterization of the Vertical Structure of Saharan Dust Export to the Mediterranean Basin, J. Geophys. Res.-Atmos., 104, 22257–22270, https://doi.org/10.1029/1999JD900257, 1999.

Hirsch, R. M., Slack, J. R., and Smith, R. A.: Techniques of Trend Analysis for Monthly Water Quality Data, Water Resour. Res., 18, 107–121, https://doi.org/10.1029/WR018i001p00107, 1982.

Hoff, R. M. and Christopher, S. A.: Remote Sensing of Particulate Pollution from Space: Have We Reached the Promised Land?, J. Air Waste Ma., 59, 645–675, https://doi.org/10.3155/1047-3289.59.6.645, 2009.

Holben, B. N., Eck, T. F., Slutsker, I., Tanré, D., Buis, J. P., Setzer, A., Vermote, E., Reagan, J. A., Kaufman, Y. J., Nakajima, T., Lavenu, F., Jankowiak, I., and Smirnov, A.: AERONET – A Federated Instrument Network and Data Archive for Aerosol Characterization, Remote Sens. Environ., 66, 1–16, 1998.

Holben, B. N., Tanré, D., Smirnov, A., Eck, T. F., Slutsker, I., Abuhassan, N., Newcomb, W. W., Schafer, J. S., Chatenet, B., Lavenu, F., Kaufman, Y. J., Vande Castle, J., Setzer, A., Markham, B., Clark, D., Frouin, R., Halthore, R., Karneli, A., O'Neill, N. T., Pietras, C., Pinker, R. T., Voss, K., and Zibordi, G.: An Emerging Ground-Based Aerosol Climatology: Aerosol Optical Depth from AERONET, J. Geophys. Res.-Atmos., 106, 12067–12097, 2001.

Huang, J., Zhang, C., and Prospero, J. M.: Large-Scale Effect of Aerosols on Precipitation in the West African Monsoon Region, Q. J Roy. Meteor. Soc., 135, 581–594, https://doi.org/10.1002/qj.391, 2009.

Ichoku, C., Chu, D. A., Mattoo, S., Kaufman, Y. J., Remer, L. A., Tanré, D., Slutsker, I., and Holben, B. N.: A Spatio-Temporal Approach for Global Validation and Analysis of MODIS Aerosol Products, Geophys. Res. Lett., 29, MOD1-1, https://doi.org/10.1029/2001GL013206, 2002.

Janicot, S.: Spatiotemporal Variability of West African Rainfall. Part II: Associated Surface and Airmass Characteristics, J. Climate, 5, 499–511, https://doi.org/10.1175/1520-0442(1992)005<0499:SVOWAR>2.0.CO;2, 1992.

Kacenelenbogen, M., Léon, J.-F., Chiapello, I., and Tanré, D.: Characterization of aerosol pollution events in France using ground-

based and POLDER-2 satellite data, Atmos. Chem. Phys., 6, 4843–4849, https://doi.org/10.5194/acp-6-4843-2006, 2006.

Kamarul Zaman, N. A. F., Kanniah, K. D., and Kaskaoutis, D. G.: Estimating Particulate Matter Using Satellite Based Aerosol Optical Depth and Meteorological Variables in Malaysia, Atmos. Res., 193, 142–162, https://doi.org/10.1016/j.atmosres.2017.04.019, 2017.

Kaskaoutis, D. G. and Kambezidis, H. D.: Comparison of the Ångström Parameters Retrieval in Different Spectral Ranges with the Use of Different Techniques, Meteorol. Atmos. Phys., 99, 233–246, https://doi.org/10.1007/s00703-007-0279-y, 2008.

Kaskaoutis, D. G., Badarinath, K. V. S., Kharol, S. K., Sharma, A. R., and Kambezidis, H. D.: Variations in the Aerosol Optical Properties and Types over the Tropical Urban Site of Hyderabad, India, J. Geophys. Res.-Atmos., 114, D22204, https://doi.org/10.1029/2009JD012423, 2009.

Kaufman, Y. J., Tanré, D., Gordon, H. R., Nakajima, T., Lenoble, J., Frouin, R., Grassl, H., Herman, B. M., King, M. D., and Teillet, P. M.: Passive Remote Sensing of Tropospheric Aerosol and Atmospheric Correction for the Aerosol Effect, J. Geophys. Res.-Atmos., 102, 16815–16830, 1997.

Kaufman, Y. J., Tanré, D., and Boucher, O.: A Satellite View of Aerosols in the Climate System, Nature, 419, 215–223, https://doi.org/10.1038/nature01091, 2002.

Kniffka, A., Knippertz, P., and Fink, A. H.: The role of low-level clouds in the West African monsoon system, Atmos. Chem. Phys., 19, 1623–1647, https://doi.org/10.5194/acp-19-1623-2019, 2019.

Knippertz, P., Evans, M. J., Field, P. R., Fink, A. H., Liousse, C., and Marsham, J. H.: The Possible Role of Local Air Pollution in Climate Change in West Africa, Nat. Clim. Change, 5, 815–822, https://doi.org/10.1038/nclimate2727, 2015.

Koren, I., Kaufman, Y. J., Washington, R., Todd, M. C., Rudich, Y., Martins, J. V., and Rosenfeld, D.: The Bodele Depression: A Single Spot in the Sahara That Provides Most of the Mineral Dust to the Amazon Forest, Environ. Res. Lett., 1, 014005, https://doi.org/10.1088/1748-9326/1/1/014005, 2006.

Lélé, M. I. and Lamb, P. J.: Variability of the Intertropical Front (ITF) and Rainfall over the West African Sudan-Sahel Zone, J. Climate, 23, 3984–4004, https://doi.org/10.1175/2010JCLI3277.1, 2010.

Léon, J.-F., Chazette, P., and Dulac, F.: Retrieval and Monitoring of Aerosol Optical Thickness over an Urban Area by Spaceborne and Ground-Based Remote Sensing, Appl. Optics, 38, 6918–6926, 1999.

Léon, J.-F., Derimian, Y., Chiapello, I., Tanré, D., Podvin, T., Chatenet, B., Diallo, A., and Deroo, C.: Aerosol vertical distribution and optical properties over M'Bour (16.96° W; 14.39° N), Senegal from 2006 to 2008, Atmos. Chem. Phys., 9, 9249–9261, https://doi.org/10.5194/acp-9-9249-2009, 2009.

Levy, R. C., Remer, L. A., Kleidman, R. G., Mattoo, S., Ichoku, C., Kahn, R., and Eck, T. F.: Global evaluation of the Collection 5 MODIS dark-target aerosol products over land, Atmos. Chem. Phys., 10, 10399–10420, https://doi.org/10.5194/acp-10-10399-2010, 2010.

Levy, R. C., Mattoo, S., Munchak, L. A., Remer, L. A., Sayer, A. M., Patadia, F., and Hsu, N. C.: The Collection 6 MODIS aerosol products over land and ocean, Atmos. Meas. Tech., 6, 2989–3034, https://doi.org/10.5194/amt-6-2989-2013, 2013.

Li, Z., Lau, W. K.-M., Ramanathan, V., Wu, G., Ding, Y., Manoj, M. G., Liu, J., Qian, Y., Li, J., Zhou, T., Fan, J., Rosenfeld, D., Ming, Y., Wang, Y., Huang, J., Wang, B., Xu, X., Lee, S.-S., Cribb, M., Zhang, F., Yang, X., Zhao, C., Takemura, T., Wang, K., Xia, X., Yin, Y., Zhang, H., Guo, J., Zhai, P. M., Sugimoto, N., Babu, S. S., and Brasseur, G. P.: Aerosol and Monsoon Climate Interactions over Asia, Rev. Geophys., 54, 866–929, https://doi.org/10.1002/2015RG000500, 2016.

Liou, K.-N.: An Introduction to Atmospheric Radiation, Vol. 84,, 2nd edn., in: International Geophysics Series, Academic Press, Amsterdam, Boston, 2002.

Liousse, C., Guillaume, B., Grégoire, J. M., Mallet, M., Galy, C., Pont, V., Akpo, A., Bedou, M., Castéra, P., Dungall, L., Gardrat, E., Granier, C., Konaré, A., Malavelle, F., Mariscal, A., Mieville, A., Rosset, R., Serça, D., Solmon, F., Tummon, F., Assamoi, E., Yoboué, V., and Van Velthoven, P.: Updated African biomass burning emission inventories in the framework of the AMMA-IDAF program, with an evaluation of combustion aerosols, Atmos. Chem. Phys., 10, 9631–9646, https://doi.org/10.5194/acp-10-9631-2010, 2010.

Liousse, C., Assamoi, E., Criqui, P., Granier, C., and Rosset, R.: Explosive Growth in African Combustion Emissions from 2005 to 2030, Environ. Res. Lett., 9, 035003, https://doi.org/10.1088/1748-9326/9/3/035003, 2014.

Lynch, P., Reid, J. S., Westphal, D. L., Zhang, J., Hogan, T. F., Hyer, E. J., Curtis, C. A., Hegg, D. A., Shi, Y., Campbell, J. R., Rubin, J. I., Sessions, W. R., Turk, F. J., and Walker, A. L.: An 11-year global gridded aerosol optical thickness reanalysis (v1.0) for atmospheric and climate sciences, Geosci. Model Dev., 9, 1489–1522, https://doi.org/10.5194/gmd-9-1489-2016, 2016.

Ma, Z., Hu, X., Sayer, A. M., Levy, R., Zhang, Q., Xue, Y., Tong, S., Bi, J., Huang, L., and Liu, Y.: Satellite-Based Spatiotemporal Trends in PM2.5 Concentrations: China, 2004–2013, Environ. Health Persp., 124, 2, https://doi.org/10.1289/ehp.1409481, 2015.

Mallet, M., Pont, V., Liousse, C., Gomes, L., Pelon, J., Osborne, S., Haywood, J., Roger, J. C., Dubuisson, P., Mariscal, A., Thouret, V., and Goloub, P.: Aerosol Direct Radiative Forcing over Djougou (Northern Benin) during the African Monsoon Multidisciplinary Analysis Dry Season Experiment (Special Observation Period-0), J. Geophys. Res., 113, D00C01, https://doi.org/10.1029/2007JD009419, 2008.

Marais, E. A., Jacob, D. J., Wecht, K., Lerot, C., Zhang, L., Yu, K., Kurosu, T. P., Chance, K., and Sauvage, B.: Anthropogenic Emissions in Nigeria and Implications for Atmospheric Ozone Pollution: A View from Space, Atmos. Environ., 99, 32–40, https://doi.org/10.1016/j.atmosenv.2014.09.055, 2014.

Mehta, M., Singh, N., and Anshumali: Global Trends of Columnar and Vertically Distributed Properties of Aerosols with Emphasis on Dust, Polluted Dust and Smoke – Inferences from 10-Year Long CALIOP Observations, Remote Sens. Environ., 208, 120–132, https://doi.org/10.1016/j.rse.2018.02.017, 2018.

Menut, L., Flamant, C., Turquety, S., Deroubaix, A., Chazette, P., and Meynadier, R.: Impact of biomass burning on pollutant surface concentrations in megacities of the Gulf of Guinea, At-

mos. Chem. Phys., 18, 2687–2707, https://doi.org/10.5194/acp-18-2687-2018, 2018.

Nakajima, T., Hayasaka, T., Higurashi, A., Hashida, G., Moharram-Nejad, N., Najafi, Y., and Valavi, H.: Aerosol Optical Properties in the Iranian Region Obtained by Ground-Based Solar Radiation Measurements in the Summer Of 1991, J. Appl. Meteorol., 35, 1265–1278, https://doi.org/10.1175/1520-0450(1996)035<1265:AOPITI>2.0.CO;2, 1996.

Ologunorisa, T. E.: A Review of the Effects of Gas Flaring on the Niger Delta Environment, Int. J. Sust. Dev. World, 8, 249–255, https://doi.org/10.1080/13504500109470082, 2001.

O'Neill, N., Ignatov, A., Holben, B. N., and Eck, T. F.: The Lognormal Distribution as a Reference for Reporting Aerosol Optical Depth Statistics; Empirical Tests Using Multi-Year, Multi-Site AERONET Sunphotometer Data, Geophys. Res. Lett., 27, 3333–3336, https://doi.org/10.1029/2000GL011581, 2000.

Ouafo-Leumbe, M.-R., Galy-Lacaux, C., Liousse, C., Pont, V., Akpo, A., Doumbia, T., Gardrat, E., Zouiten, C., Sigha-Nkamdjou, L., and Ekodeck, G. E.: Chemical Composition and Sources of Atmospheric Aerosols at Djougou (Benin), Meteorol. Atmos. Phys., 130, 591–609, https://doi.org/10.1007/s00703-017-0538-5, 2017.

Perrone, M., Santese, M., Tafuro, A., Holben, B., and Smirnov, A.: Aerosol Load Characterization over South–East Italy for One Year of AERONET Sun-Photometer Measurements, Atmos. Res., 75, 111–133, https://doi.org/10.1016/j.atmosres.2004.12.003, 2005.

Porter, J. N., Miller, M., Pietras, C., and Motell, C.: Ship-Based Sun Photometer Measurements Using Microtops Sun Photometers, J. Atmos. Ocean. Tech., 18, 765–774, 2001.

Prospero, J., Savoie, D., Carlson, T., and Nees, R.: Saharan Aerosol Transport by Means of Atmospheric Turbidity Measurements, in: Saharan Dust Mobilization, Transport, Deposition, vol. 14, chap. 8, John Wiley, San Diego, Calif., 171–186, 1979.

Prospero, J. M. and Nees, R. T.: Dust Concentration in the Atmosphere of the Equatorial North Atlantic: Possible Relationship to the Sahelian Drought, Science, 196, 1196–1198, https://doi.org/10.1126/science.196.4295.1196, 1977.

Redelsperger, J.-L., Thorncroft, C. D., Diedhiou, A., Lebel, T., Parker, D. J., and Polcher, J.: African Monsoon Multidisciplinary Analysis: An International Research Project and Field Campaign, B. Am. Meteorol. Soc., 87, 1739–1746, https://doi.org/10.1175/BAMS-87-12-1739, 2006.

Remer, L. A., Kaufman, Y. J., Tanré, D., Mattoo, S., Chu, D. A., Martins, J. V., Li, R.-R., Ichoku, C., Levy, R. C., Kleidman, R. G., Eck, T. F., Vermote, E., and Holben, B. N.: The MODIS Aerosol Algorithm, Products, and Validation, J. Atmos. Sci., 62, 947–973, https://doi.org/10.1175/JAS3385.1, 2005.

Remer, L. A., Kleidman, R. G., Levy, R. C., Kaufman, Y. J., Tanré, D., Mattoo, S., Martins, J. V., Ichoku, C., Koren, I., Yu, H., and Holben, B. N.: Global Aerosol Climatology from the MODIS Satellite Sensors, J. Geophys. Res., 113, D14S07, https://doi.org/10.1029/2007JD009661, 2008.

Remer, L. A., Levy, R. C., Mattoo, S., Tanré, D., Gupta, P., Shi, Y., Sawyer, V., Munchak, L. A., Zhou, Y., Kim, M., Ichoku, C., Patadia, F., Li, R.-R., Gassó, S., Kleidman, R. G., and Holben, B. N.: The Dark Target Algorithm for Observing the Global Aerosol System: Past, Present, and Future, Remote Sens.-Basel, 12, 2900, https://doi.org/10.3390/rs12182900, 2020.

Ruiz-Arias, J. A., Dudhia, J., Gueymard, C. A., and Pozo-Vázquez, D.: Assessment of the Level-3 MODIS daily aerosol optical depth in the context of surface solar radiation and numerical weather modeling, Atmos. Chem. Phys., 13, 675–692, https://doi.org/10.5194/acp-13-675-2013, 2013.

Sayer, A. M., Hsu, N. C., Bettenhausen, C., and Jeong, M.-J.: Validation and Uncertainty Estimates for MODIS Collection 6 "Deep Blue" Aerosol Data, J. Geophys. Res.-Atmos., 118, 7864–7872, https://doi.org/10.1002/jgrd.50600, 2013.

Sayer, A. M., Munchak, L. A., Hsu, N. C., Levy, R. C., Bettenhausen, C., and Jeong, M.-J.: MODIS Collection 6 Aerosol Products: Comparison between Aqua's e-Deep Blue, Dark Target, and "Merged" Data Sets, and Usage Recommendations, J. Geophys. Res.-Atmos., 119, 13965–13989, https://doi.org/10.1002/2014JD022453, 2014.

Sayer, A. M., Hsu, N. C., Hsiao, T.-C., Pantina, P., Kuo, F., Ou-Yang, C.-F., Tsay, S.-C., Holben, B. N., Janjai, S., Chantara, S., Wang, S.-H., Loftus, A. M., and Lin, N.-H.: In-Situ and Remotely-Sensed Observations of Biomass Burning Aerosols at Doi Ang Khang, Thailand during 7-SEAS/BASELInE 2015, Aerosol Air Qual. Res., 16, 2786–2801, https://doi.org/10.4209/aaqr.2015.08.0500, 2016.

Sayer, A. M., Hsu, N. C., Lee, J., Kim, W. V., and Dutcher, S. T.: Validation, Stability, and Consistency of MODIS Collection 6.1 and VIIRS Version 1 Deep Blue Aerosol Data Over Land, J. Geophys. Res.-Atmos., 124, 4658–4688, https://doi.org/10.1029/2018JD029598, 2019.

Schepanski, K., Tegen, I., and Macke, A.: Saharan dust transport and deposition towards the tropical northern Atlantic, Atmos. Chem. Phys., 9, 1173–1189, https://doi.org/10.5194/acp-9-1173-2009, 2009.

Schmid, B. and Wehrli, C.: Comparison of Sun Photometer Calibration by Use of the Langley Technique and the Standard Lamp, Appl. Optics, 34, 4500, https://doi.org/10.1364/AO.34.004500, 1995.

Sharma, M., Kaskaoutis, D. G., Singh, R. P., and Singh, S.: Seasonal Variability of Atmospheric Aerosol Parameters over Greater Noida Using Ground Sunphotometer Observations, Aerosol Air Qual. Res., 14, 608–622, https://doi.org/10.4209/aaqr.2013.06.0219, 2014.

Sinha, P. R., Gupta, P., Kaskaoutis, D. G., Sahu, L. K., Nagendra, N., Manchanda, R. K., Kumar, Y. B., and Sreenivasan, S.: Estimation of Particulate Matter from Satellite- and Ground-Based Observations over Hyderabad, India, Int. J. Remote Sens., 36, 6192–6213, https://doi.org/10.1080/01431161.2015.1112929, 2015.

Smirnov, A.: Diurnal Variability of Aerosol Optical Depth Observed at AERONET (Aerosol Robotic Network) Sites, Geophys. Res. Lett., 29, 2115, https://doi.org/10.1029/2002GL016305, 2002.

Smirnov, A., Holben, B. N., Eck, T. F., Dubovik, O., and Slutsker, I.: Cloud-Screening and Quality Control Algorithms for the AERONET Database, Remote Sens. Environ., 73, 337–349, https://doi.org/10.1016/S0034-4257(00)00109-7, 2000.

Soufflet, V., Devaux, C., and Tanré, D.: Modified Langley Plot Method for Measuring the Spectral Aerosol Optical Thickness and Its Daily Variations, Appl. Optics, 31, 2154, https://doi.org/10.1364/AO.31.002154, 1992.

Tanré, D., Deschamps, P. Y., Devaux, C., and Herman, M.: Estimation of Saharan Aerosol Optical Thickness from Blurring Effects

in Thematic Mapper Data, J. Geophys. Res.-Atmos., 93, 15955–15964, https://doi.org/10.1029/JD093iD12p15955, 1988.

Todd, M. C., Washington, R., Martins, J. V., Dubovik, O., Lizcano, G., M'Bainayel, S., and Engelstaedter, S.: Mineral Dust Emission from the Bodélé Depression, Northern Chad, during BoDEx 2005, J. Geophys. Res., 112, D06207, https://doi.org/10.1029/2006JD007170, 2007.

Toledano, C., Cachorro, V. E., Berjon, A., de Frutos, A. M., Sorribas, M., de la Morena, B. A., and Goloub, P.: Aerosol Optical Depth and Ångström Exponent Climatology at El Arenosillo AERONET Site (Huelva, Spain), Q. J. Roy. Meteor. Soc., 133, 795–807, https://doi.org/10.1002/qj.54, 2007.

van Donkelaar, A., Martin, R. V., Brauer, M., Kahn, R., Levy, R., Verduzco, C., and Villeneuve, P. J.: Global Estimates of Ambient Fine Particulate Matter Concentrations from Satellite-Based Aerosol Optical Depth: Development and Application, Environ. Health Persp., 118, 847–855, https://doi.org/10.1289/ehp.0901623, 2010.

van Donkelaar, A., Martin, R. V., Brauer, M., Hsu, N. C., Kahn, R. A., Levy, R. C., Lyapustin, A., Sayer, A. M., and Winker, D. M.: Global Estimates of Fine Particulate Matter Using a Combined Geophysical-Statistical Method with Information from Satellites, Models, and Monitors, Environ. Sci. Technol., 50, 3762–3772, https://doi.org/10.1021/acs.est.5b05833, 2016.

Verma, S.: A New Classification of Aerosol Sources and Types as Measured over Jaipur, India, Aerosol Air Qual. Res., 15, 985–993, https://doi.org/10.4209/aaqr.2014.07.0143, 2015.

Volz, F.: Photometer Mit Selen-Photoelement Zur Spektralen Messung Der Sonnenstrahlung Und Zur Bestimmung Der Wellenlängenabhängigkeit Der Dunsttrübung, Arch. Meteor. Geophy. B, 10, 100–131, https://doi.org/10.1007/BF02243122, 1959.

Volz, F. E.: Economical Multispectral Sun Photometer for Measurements of Aerosol Extinction from 0.44 Mm to 1.6 Mm and Precipitable Water, Appl. Optics, 13, 1732–1733, 1974.

Wagner, F. and Silva, A. M.: Some considerations about Ångström exponent distributions, Atmos. Chem. Phys., 8, 481–489, https://doi.org/10.5194/acp-8-481-2008, 2008.

Washington, R.: Atmospheric Controls on Mineral Dust Emission from the Bodélé Depression, Chad: The Role of the Low Level Jet, Geophys. Res. Lett., 32, 17, https://doi.org/10.1029/2005GL023597, 2005.

Wei, J., Peng, Y., Guo, J., and Sun, L.: Performance of MODIS Collection 6.1 Level 3 Aerosol Products in Spatial-Temporal Variations over Land, Atmos. Environ., 206, 30–44, https://doi.org/10.1016/j.atmosenv.2019.03.001, 2019.

Yahi, H., Marticorena, B., Thiria, S., Chatenet, B., Schmechtig, C., Rajot, J. L., and Crepon, M.: Statistical Relationship between Surface PM10 Concentration and Aerosol Optical Depth over the Sahel as a Function of Weather Type, Using Neural Network Methodology, J. Geophys. Res.-Atmos., 118, 13265–13281, https://doi.org/10.1002/2013JD019465, 2013.

Yang, Q., Yuan, Q., Yue, L., Li, T., Shen, H., and Zhang, L.: The Relationships between PM2.5 and Aerosol Optical Depth (AOD) in Mainland China: About and behind the Spatio-Temporal Variations, Environ. Pollut., 248, 526–535, https://doi.org/10.1016/j.envpol.2019.02.071, 2019.

Yoon, J.-H., Rasch, P. J., Wang, H., Vinoj, V., and Ganguly, D.: The Role of Carbonaceous Aerosols on Short-Term Variations of Precipitation over North Africa, Atmos. Sci. Lett., 17, 407–414, https://doi.org/10.1002/asl.672, 2016.

Zheng, C., Zhao, C., Zhu, Y., Wang, Y., Shi, X., Wu, X., Chen, T., Wu, F., and Qiu, Y.: Analysis of influential factors for the relationship between $PM_{2.5}$ and AOD in Beijing, Atmos. Chem. Phys., 17, 13473–13489, https://doi.org/10.5194/acp-17-13473-2017, 2017.